# Gold Nanoparticle-Based Laser Photothermal Therapy

Navid Manuchehrabadi and Liang Zhu

**Abstract**

Laser photothermal therapy using gold nanoparticles in cancer research has attracted a lot of attentions in past decades, since it provides an alternative approach to traditional hyperthermia methods. This review is focused on advancements in gold nanoparticle development and the underlying mechanisms to confine heat generation in tumors when these nanoparticles interact with an incident laser. First, an overview of hyperthermia used in medicine is given, and the development of gold nanoparticles in laser photothermal therapy is discussed. Second, physical mechanisms in generating heat utilizing gold nanoparticles, nanoparticle delivery, and toxicity reaction after injection are described. The next section is focused on evaluation of performance of laser photothermal therapy in clinical/animal studies. Monte Carlo methods are presented to demonstrate current theoretical simulation approaches to determine laser energy absorption distribution in tissue enhanced by gold nanoparticles. Furthermore, modeling heat transfer and assessing thermal damage in biological tissue using gold nanoparticles in designing treatment protocols are described to show a typical designing process. At the end of this review, the current challenges facing clinicians and researchers in delivering effective and safe thermal dosage in laser photothermal therapy are discussed.

N. Manuchehrabadi
Department of Mechanical Engineering, University of Minnesota at Minneapolis, Minneapolis, MN, USA
e-mail: manuc001@umn.edu

L. Zhu (✉)
Department of Mechanical Engineering, University of Maryland Baltimore County, Baltimore, MD, USA
e-mail: zliang@umbc.edu



F.A. Kulacki (ed.), *Handbook of Thermal Science and Engineering*,
DOI 10.1007/978-3-319-32003-8_69-1

## Contents



## 1 Introduction

Cancer claims lives of more than half a million Americans each year. Based on the annual report of the American Cancer Society, cancer is the second leading cause of death in the United States, exceeded only by heart disease. The 5-year survival rate for all cancers diagnosed between 2005 and 2011 is 69%, up from 49% in the 1970s. The improvement in the 5-year survival rate of cancer patients may be due to progress in cancer diagnosis as well as numerous innovations in cancer treatment (American Cancer Society 2016). Surgery (open, laparoscopic, or robotic-assisted), external beam radiation, or radioactive seed implants (brachytherapy) may be used to treat tumors at their early stages. Hormonal therapy, chemotherapy, radiation, thermal therapy, and combinations of these approaches are used to treat cancer at later stages.

Hyperthermia is defined as any treatment or technique that elevates tissue temperature for a specific time duration to achieve an ultimate therapeutic goal. Hyperthermia includes mild hyperthermia, acute hyperthermia, and tissue coagulation or ablation. Mild hyperthermia (from 39 °C to 43 °C) is usually used as an adjuvant therapy with radiation or chemotherapy because it causes cells to be susceptible to ionizing radiation therapy or chemotherapy drugs (Issels et al. 2010; Werthmöller et al. 2016). Acute hyperthermia (43–48 °C) can produce reversible injury and dysfunction or irreversible damage, leading to immediate or programmed cell death (Pearce 2009). Tissue ablation and coagulation therapies are related to elevating cell temperatures much higher than 49 °C. At these temperature levels, heating time can be shortened significantly. Currently available hyperthermia approaches include radio frequency, microwave, ultrasound, laser, etc.

One of the downsides of the available hyperthermia techniques in cancer treatment is low spatial selectivity in heating tumors while protecting surrounding

healthy tissues from thermal damage (Berlien 2003; Tuchin 2015). In the past 10 years, gold nanoparticle-mediated laser photothermal therapy has been developed and evaluated as a promising diagnostic and therapeutic approach in cancer treatment to overcome the limitations of the traditional hyperthermia methods. For many years, gold has been used in in vivo applications for treating rheumatoid arthritis (Aaseth et al. 1998). Plasmonic photothermal therapy in recent years is an approach when metallic (gold) nanoparticles are exposed to laser irradiation near its plasmon-resonant absorption band, to activate and deactivate electrons. The unique and easily tunable optical properties of gold nanoparticles with different shapes and structures such as nanospheres (Link and El-Sayed 1999; Heilmann and Kreibig 2000; Sönnichsen et al. 2002; Hirsch et al. 2003), nanorods (Ying et al. 1997; Link et al. 1999; Jana et al. 2001; Nikoobakht and El-Sayed 2003; Pérez-Juste et al. 2005; Huang et al. 2006; Niidome et al. 2006; Huff et al. 2007; Dickerson et al. 2008; Moon et al. 2015), nanocages (Skrabalak et al. 2008; Yavuz et al. 2009), nanoprism (Millstone et al. 2005; Guo et al. 2010), nanowire (Heilmann and Kreibig 2000; Sönnichsen et al. 2002), composite nanoparticles with core and shell structure (Kang and Taton 2005; Lu et al. 2016), and nanoparticles with core and assemblies (Westcott et al. 1998; Li et al. 2002; Liang et al. 2003) may confine laser energy to targeted tumors. By carefully designing the size, shape, and structure of gold nanoparticles, one can achieve a desired absorption-scattering ratio in the therapeutic optical window (750–1100 nm) to maximize laser energy confinement in tumors (Oldenburg et al. 1998; Boris et al. 2006; Myroshnychenko et al. 2008). Previous experimental and theoretical studies have shown the effectiveness of laser photothermal therapy in cancer treatment both in tissue cultures and implanted tumors in mice (Loo et al. 2005; Gobin et al. 2008; Lal et al. 2008; Stern et al. 2008; Manuchehrabadi et al. 2012). Successful treatment outcomes are illustrated by shrinkage of tumors following the therapy, as well as observed tumor cell death in tissue culture (Manuchehrabadi et al. 2013b).

This review is focused on research advancement in the field of laser photothermal therapy for cancer treatment. An overview of the history of hyperthermia treatment for cancer is given first. The next section describes different types of gold nanoparticles and physical mechanisms of heat generation when nanoparticles interact with laser light, as well as nanoparticle delivery approaches in biological tissue. Previous researches using gold nanorods or nanoshells in laser photothermal therapy in in vitro and in vivo animal studies are discussed in the next section. A general review of theoretical modeling to simulate laser propagation in tissue using Monte Carlo methods then follows. Theoretical modeling approaches in bioheat transfer, their accuracy and limitations, and assessment of thermal damage are the focus of the next two sections to show typical procedures to design heating protocols. The review ends with future research directions that can be implemented to improve our understanding of implementing laser photothermal therapy for cancer patients.

## 2 History and Development of Hyperthermia Treatment Methods

Since the first paper on hyperthermia was published in 1886 (Bush 1886), hyperthermia has been extensively evaluated in a variety of therapeutic procedures, as either a singular therapy or an adjuvant therapy, to increase the sensitivity of cells to radiation and chemotherapy in cancer treatments (Engin 1994; Moroz et al. 2002). In the past decades, growing evidence has suggested the promise of hyperthermia for killing cancer cells. Hyperthermia is preferred for patients diagnosed with surgically complex tumors or for patients looking for an alternative to surgeries. It has been demonstrated that thermal energy delivered to tumors to raise intratumoral temperatures above 43 °C for a duration of approximately several hours causes irreversible cell damage. Adequate exposure of biological tissue to an elevated temperature may produce heat-induced cytotoxic responses and/or increase the cytotoxic effects of radiation and drugs, leading to structural dysfunction of cell protein, rupture and fragmentation of mitochondrial membrane, gradual loss of repair enzyme function, damage of membrane integrity and function, and denaturation of DNA (Bernardi et al. 2008; Kim et al. 2010; Shoshan-Barmatz et al. 2006). These ultimately cause apoptosis, necrosis, and coagulation of tumor cells (Johannsen et al. 2005; Moroz et al. 2002).

Traditional hyperthermia methods include radio frequency (RF), microwave, laser, and ultrasound. Clinical evidence (Wong et al. 2010) suggests that RF ablation has high success rates in patients with colorectal cancer, with only a few unresectable hepatic metastases (<30 mm diameter). In these patients, the 5-year survival rates varied from 14% to 55%. A study (Zou et al. 2010) using RF for unresectable pancreatic cancer indicated a marked decrease in pain score and improvements in patients. For prostate cancer treatment, local hyperthermia has been considered minimally invasive due to transurethral or transrectal access to the prostate. The effect of RF ablation was examined in another clinical study (Lanuti et al. 2009) for treating inoperable lung cancer, and it has shown 78 % and 47 % survival rates after 2 years and 4 years, respectively. It has been reported that focused ultrasound has achieved 66–80% success rates in destroying tumors (Gelet et al. 2000; Chaussy and Thüroff 2004). Another hyperthermia approach uses microwaves to elevate tumor temperatures in the prostate. The microwaves are emitted from an antenna inserted in the prostatic urethra (Neilson et al. 1994; Rudie et al. 1996; Larson et al. 1998; Sherar et al. 2001). These clinical and animal studies provide strong rationales for using hyperthermia approaches to eradicate cancer cells. Direct cellular death caused by either hyperthermia or increasing the cellular susceptibility for adjuvant treatments is strongly dependent on the achieved distribution of the temperature elevations in tumors and duration of heating. Some of the complications associated with traditional hyperthermia methods may be due to poorly designed heating protocols.

All the abovementioned hyperthermia approaches require a wave or current to be passed through tissue; when this wave or current interacts with molecules in the tissue, heat is generated. However, microwave or RF current decays as it passes through the tissue, resulting in an energy generation rate that decays rapidly from the

location where it is initiated. In addition, thermal damage to healthy tissue may occur along the paths of the wave or current. In recent years, various technology (Bernardi et al. 2008; Gobin et al. 2008; Melancon et al. 2008) have been investigated to show that gold nanoshells or nanorods injected into tumors can serve as strong laser energy absorbers, therefore, to confine laser energy in tumors, with minimal collateral damage to their surrounding healthy tissue.

## 3 Gold Nanoparticle Design for Laser Photothermal Therapy Applications

Currently, different types of gold nanoparticles are studied as imaging contrast agents, (Connor et al. 2005; Chen et al. 2013; Zhang et al. 2015; Cheheltani et al. 2016), absorptive heating agents (Hirsch et al. 2003; El-Sayed et al. 2006; Jain et al. 2006, 2012; Cherukuri et al. 2010), and dual imaging and therapeutic agents (Loo et al. 2005; Huang et al. 2006; Gobin et al. 2008; Yang et al. 2013). In recent years, laser photothermal therapy using gold nanoshells or gold nanorods has emerged as a promising therapeutic method due to its ability to deliver and confine adequate thermal dosage to tumors while minimizing laser energy absorption in surrounding healthy tissue. Various studies (Loo et al. 2005; Bernardi et al. 2008; Gobin et al. 2008; Melancon et al. 2008) have demonstrated that the geometrical parameters of gold nanoshells or nanorods can be tuned to obtain a high absorptivity at a specific laser wavelength and to serve as strong laser energy absorbers in tumors. The strong absorption is due to optical resonances of gold when its size is much smaller than the visible light wavelength (Skrabalak et al. 2008; Lal et al. 2008). Key factors to be considered when selecting nanoparticles in laser photothermal therapy are the wavelength of the maximal absorption, the spectral bandwidth, and the size of the nanoparticles (Kennedy et al. 2011).

### 3.1 Gold-Silica Nanoshells

Gold-silica nanoshells were first developed in 2003 (Hirsch et al. 2003). They are composed of a silica dielectric core coated by a thin metallic (gold) shell. Westcott et al. (1998) have shown how gold-silica nanoshells are fabricated by attachment of seeds of gold colloid to a silica core and to cover the shell via adding gold. Silica colloids are a convenient dielectric core, as they can grow with relatively controlled heterogeneity of particle sizes.

A variety of approaches has been developed for the synthesis of gold nanoshells, mainly including photochemical (Kim et al. 2002) and seed-medicated growth methods (Nikoobakht and El-Sayed 2003; Murphy et al. 2005; Ye et al. 2012). The seed-medicated growth method has been the most widely used due to its simplicity, high quality, and ease on particle size controlling. In the seed-medicated approach, gold-based nanoparticles with different aspect ratios can be produced from preformed colloidal gold seeds in a bulk $HAuCl_4$ growth solution. A growth solution

is prepared by reducing auric acid in cetyltrimethylammonium bromide (CTAB) and benzyldimethyl hexadecylammonium chloride (BDAC). Then silver salt is added to the growth solution and mixed well followed by addition of ascorbic acid with stirring to reduce $HAuCl_4$ to $HAuCl_2$ growth solution. Eventually, the seed solution is introduced into the growth solution, and the solution can sit still for gold nanolayers to grow. The ascorbic acid reduces $Au^+$ to $Au^0$ on the surface of gold nanoparticles due to autocatalysis (Nikoobakht and El-Sayed 2003). The size and ratio of gold to silicon core can be controlled by many parameters such as seed concentration, seed size, citrate/gold ratio, reductant concentration, temperature, pH, and gold concentration and surfactant concentration. Generally, smaller amounts of reductant yield larger nanospheres (Cai et al. 2008). A PEG surface coating to the obtained gold nanostructure ensures their stability against agglomeration in physiological conditions (Zaman et al. 2007; Kogan et al. 2008).

The size of spherical gold nanoshells varies from 1.8 to 125 nm in diameter. With an increase in the particle size, the absorption peak shifts to a longer wavelength (Millstone et al. 2005). The higher-order modes in the field expansion become more important as the nanoparticle becomes larger. This results in the appearance of quadrupole resonances and possibly octopole peaks for very large particles. In practice, varying the ratio of the gold layer thickness to the silica core radius is a feasible approach to shift the absorption peak to a desirable wavelength. As showed in the study by Millstone et al. (2005), the peaks shift to the red and become intense as the shell thickness decreases.

In hyperthermia applications, metallic electrons resonantly oscillate and dissipate energy as heat when subject to laser irradiation at a specific laser wavelength. Silica-based gold nanoshells have been broadly tested in in vitro experiments in cancer therapy for human breast (Hirsch et al. 2003; Lal et al. 2008; Zhang et al. 2011, 2013; Joshi et al. 2012), prostate (Stern et al. 2008, 2016; Gobin et al. 2008), brain (Madsen et al. 2006; Bernardi et al. 2008; Meyers et al. 2015), pulmonary (Noh et al. 2015), and liver (Liu et al. 2010; Ashokkumar et al. 2014; Zhang et al. 2016a) cancers. In addition, nanoshell-mediated photothermal therapy has shown efficacy against xenografted subcutaneous tumors in mice and allografted tumors in dogs (O'Neal et al. 2004; Schwartz et al. 2009). Although a study (Madsen et al. 2012) has shown the ability of gold-silica nanoshells to be readily phagocytosed by macrophages without any toxic effects in their in vitro study in human glioma spheroids, the larger size of gold nanoshells is a big challenge for some applications especially in treatment for malignant glioma. This challenge arises due to the blood-brain barrier, which prevents entry of most therapeutic agents having a size similar to gold nanoshells into the brain (Madsen et al. 2012).

## 3.2 Gold Nanorods

Gold nanorods are made of pure gold. They can be manufactured using electrochemical (Pérez-Juste et al. 2005), photochemical (Kim et al. 2002), template (Martin 1994), and seed-medicated growth methods (Nikoobakht and El-Sayed

2003; Murphy et al. 2005; Ye et al. 2012). Gold nanorods exhibit transverse and longitudinal surface plasmon resonances that correspond to electron oscillations perpendicular and parallel to the rod length direction, respectively. Gold nanorods can be easily tuned to the near-infrared (NIR) region by simple manipulation of their aspect ratio. Compared to gold nanoshells, gold nanorods have the advantage of smaller sizes (10 nm transversal $\times$ 50 nm longitudinal), higher absorptivity, and narrower spectral bandwidths due to smaller polydispersion in their size.

Both experimental and theoretical results have demonstrated the ability of gold nanorods to offer a superior absorption of laser energy compared to gold-silica nanoshells. The laser absorption rate per gram of gold of nanorods is at least six times higher than other gold colloids (Jain et al. 2006; von Maltzahn et al. 2009; Cole et al. 2009). Compared to other conventional light absorption dyes, its absorption and scattering rates are several orders of magnitude larger (Jain et al. 2006). Furthermore, the tunability to enhance scattering and absorption in the longitudinal surface plasmon wavelength allows gold nanorods to serve as composite material with hydrogel (Krag et al. 2002; Gorelikov et al. 2004), polymer (Pérez-Juste et al. 2005; Murphy et al. 2005), silica (Chon et al. 2007), and bacteria (Berry et al. 2005). Gold nanorods also offer advantages of good biocompatibility, facile preparation, and good conjugation with different bimolecular ligands, antibodies, and other targeting moieties (Katz and Willner 2004). A major challenge in using gold nanorods in laser photothermal therapy applications is their tendency to reshape into gold nanospheres under intense laser irradiation. This may result in loss in their longitudinal resonance and reduction of their energy absorption rate. Like silica-gold nanoshells, gold nanorods have been studied in applications including laser photothermal therapy, biochemical sensing, medical diagnosis, therapeutics, enhanced imaging contrast agent in dark field microscopy, and two-photon microscopy (Engin 1994; Ying et al. 1997; Link et al. 1999; Link and El-Sayed 1999; Jana et al. 2001; Kim et al. 2002; Nikoobakht and El-Sayed 2003; Pérez-Juste et al. 2005; Huang et al. 2006; Dickerson et al. 2008; Maltzahn et al. 2009; Yang et al. 2013; Zhang et al. 2013; von Gong et al. 2013; Mercatelli et al. 2013; Manuchehrabadi et al. 2013b; Moon et al. 2015).

## 3.3 Gold Nanorods/Nanospheres Excitation Mechanisms

Laser is an electromagnetic wave, which has both electric and magnetic components, perpendicular to each other and perpendicular to the direction of energy and wave propagations. In the presence of an oscillating electromagnetic field of laser light, the conduction band of electrons of the metallic nanoparticle undergoes a collective coherent resonant oscillation with respect to surface plasmon oscillation. This requires that the natural frequency of the surface plasmon resonance matches the frequency of the incident light; this phenomenon is called surface plasmon resonance (SPR). The frequency of SPR oscillation depends on the size, shape, surrounding medium, and dielectric constant of the nanoparticles (Huang et al. 2011). The

induced surface plasmon oscillations decay either by radiative or non-radiative decay. In radiative decay the absorbed light energy causes phonon emission at the same frequency as the incident light, called Mie or Rayleigh scattering (Mie 1908). This strong light scattering property of gold nanorods in the NIR region makes them potential candidates for noninvasive imaging techniques in the NIR band. The non-radiative decay occurs via electron-hole recombination. The energy exchange mechanism has two phases: electron-phonon interaction and phonon-phonon interaction. The excited electrons cool off rapidly by energy exchange with the nanoparticles in less than a picosecond, resulting in a hot particle lattice (Link and El-Sayed 2000; Link et al. 2000). The hot particle lattice exchanges this energy with the surrounding medium within 100 picoseconds via phonon-phonon interaction. Such rapid energy exchange and strongly induced heat dissipation are desirable in hyperthermia applications.

Gold nanorods have two SPRs. For example, one strong absorption band around 800 nm is induced by electron oscillations along the longitudinal direction, and the other weaker absorption in the visible bandwidth around 500 nm is triggered along the transversal direction. Energy absorption by gold nanorods is very sensitive to the aspect ratio of the longitudinal to the transversal diameters. In a study by Ng and Cheng (2012), it is found that with an increase in the aspect ratio from 2.4 to 6.6, the maximum surface plasmon resonance shifts from the visible range (~550 nm) to the near-infrared range (~700 nm).

Laser photothermal therapy requires sufficient penetration of the laser energy through the superficial tissue and then adequate accumulation of laser absorption within the targeted tumor region. Among all the wavelengths of available lasers, the near-infrared (NIR) range has the advantage of maximal transmissivity in normal tissue over other wavelengths. It has been suggested that an NIR laser with a wavelength of approximately 800 nm may penetrate into normal tissue with minimal laser absorption before reaching the targeted tumor with deposition of gold nanorods (Vogel and Venugopalan 2003).

In non-turbid tissues, optical transmission can be modeled by the Beer-Lambert's law (Welch and van Germert 1995), and the amount of the deposited laser energy decays exponentially with depth. In the absence of scattering, the reciprocal of the absorption coefficient $\mu_a[\mathrm{cm}^{-1}]$ defines the optical penetration depth $\delta = (1/\mu_a)$ [cm] and thus the characteristic length of laser energy deposition. The optical window is referred here as the absorption dip on the curves of hemoglobin and oxyhemoglobin (Hb and $HbO_2$) around 700–800 nm wavelength (Vogel and Venugopalan 2003). Therefore, combined with a very low absorption coefficient of water, the equivalent of the absorption coefficient of human tissue would appear almost "transparent" to the 800 nm laser light before the laser reaches the nanostructures in tumors, which minimizes the heating in nontarget tissues. Due to the powerful optical absorption by nanorods, laser energy is concentrated in an area congregating by nanorods, and then the energy absorbed can be transferred to the surrounding tumor tissue by heat conduction. Fiber optic probes have been used to provide facile and inexpensive laser energy delivery to deep-seated tumors.

## 3.4 Gold Nanoparticle Delivery

One of the key issues in any hyperthermia therapy approaches is the delivery of nanoparticles to a targeted region. Inadequate accumulation of nanoparticles can cause inadequate heating in tumor tissue, leading to failure of therapy. In addition, gold nanoparticles deposited in tumors may only be a small percentage of the initially injected dosage, and the majority of the injected nanoparticles may be trapped in nontargeted organs such as the liver and spleen. Gold nanoparticles can be delivered either with direct intratumoral injections or by systemic administration. In a systemic delivery, nanoparticle accumulation is attributed to the enhanced permeability of the angiogenic tumor vasculature, which is malformed compared to normal blood vessel structures (Decuzzi et al. 2008). The size of particles and stage of tumor growth are two key factors affecting permeability of blood vessels in a tumor region. Tumors at early stages may have smaller fenestrations; therefore, the passage of nanoparticles in those tumors is harder. Another challenge in nanoparticle delivery is to achieve a homogenous distribution of nanoparticles through the entire tumor region, since bulk accumulation of nanoparticles may be confined into isolated locations.

Most nanoparticles developed for medical applications are coated with polyethylene glycol (PEG) favoring targeted delivery to a tumor (Harris and Chess 2003; Roberts et al. 2012). The increase in the hydrodynamic particle size with a coating also reduces nanoparticle filtration through the spleen and liver, therefore increasing the circulation time of nanoparticles in the bloodstream (Bazile et al. 1995; Peracchia et al. 1999; Niidome et al. 2006; Zhang et al. 2009). Zhang et al. (2009) reported that a systemic injection in mice with 20 nm PEG-coated gold nanospheres showed slower clearance of nanoparticles and less uptake in the reticuloendothelial system and a longer circulation time than that when using nanoparticles of similar sizes without coating.

Many researchers suggested utilization of tumor-specific markers to bind nanoparticles directly to specific cancer cells. In in vitro studies by Loo et al. (2005), they modified gold-silica nanoshells with antibody targeting breast cancer receptors, the human epidermal growth factor receptor 2 (HER2). The enhanced specificity of antibody targeting has been demonstrated with several other antibodies in vitro, including anti-EGFR conjugated with gold nanorods, and antibodies for acute lymphoblastic leukemia and medulloblastoma (Huang et al. 2006; Bernardi et al. 2008; Norman et al. 2008). Black et al. (2008) used gold nanorods conjugated to modified deltorphin peptide. Tong et al. (2007) demonstrated that folate-conjugated nanorods have enhanced laser absorption in tumor regions compare to bare gold nanorods. An in vivo study by Melancon et al. (2008) utilized modified hollow gold nanoshells with anti-EGFR (anti-epidermal growth factor receptor). Histological analyses were performed to confirm a significant increase in the nanoshell delivery to targeted tumors.

New study showed the effect of a pH-sensitive linker multifunctional gold nanorod system (GNR-Dox-Tf-NP), which can selectively target and deliver Dox to lung tumor cells and alleviate free Dox-mediated toxicity to normal cells

(Amreddy et al. 2015). Very similar approaches were suggested by another group showing that the nanomedicine can rapidly and effectively release its Dox payload triggered by an acidic pH environment (pH ~ 5) and/or an 808 nm NIR laser irradiation (Zhang et al. 2016b).

Another improvement was suggested to suppress the fundamental cellular defense mechanism of heat shock response, which leads to therapeutic resistance of cancer cells and reduces the therapeutic efficacy. Wang et al. (2016) introduced a gold nanorod-siRNA platform with gene silencing capability to improve photothermal therapy efficiency. A new study performed by Zhang et al. (2009) implied that the toxicity derived from CTAB during gold nanorod synthesis can severely limit their medical applications. However, they reported a novel idea of synthesizing polyethyleneimine (PEI)-coated gold nanorods to improve the biocompatibility and siRND delivery in laser photothermal therapy (Zhang et al. 2009).

An alternative strategy in systemic delivery utilizes large microparticles to transport nanoparticles to targeted tumors with the rationale that these larger microparticles will minimally accumulate in nontargeted organs such as the liver and spleen (Kennedy et al. 2011). In this approach, microparticles are loaded with therapeutic nanoparticles and delivered to tumor vasculature. Once they reach the tumor vicinity, the nanoparticles diffuse out of the microparticles through the nanoscale porous structures there. Tasciotti et al. (2008) have developed this strategy via injecting intravenously 3–4 μm gold-silica microparticles. They demonstrated that the microparticles could carry carbon nanotubes to cancer cell cytosols. Another vehicular approach is called "Trojan horse," in which gold-silica nanoshells incubate with macrophage cells for 24 h and are taken via phagocytosis (Choi et al. 2007). Then, the loaded macrophages are unloaded to tumors. The nanoshell-loaded macrophages finally passed the tumor spheroids and accumulated at the rim of the spheroid's core hypoxic region.

It has been suggested that surface charge of nanoparticles may affect the distribution of gold nanoparticles in tumors. One study has shown that positively charged nanoparticles are efficiently endocytosed by tumors, while negatively charged nanoparticles spread rapidly throughout the bulk of tumors (Kim et al. 2010). By changing the surface charge from negative to positive, it has been shown that the polylactic-co-glycolic acid (PLGA) nanoparticles pass the endosomes and reach the cytoplasm, rather than being confined in lysosomes. Another way to modify gold nanoparticle delivery involves application of a novel noncytotoxic antimicrobial contraceptive agent called polystyrene sulfonate (PSS) polyelectrolyte (Garg et al. 2005; Durr et al. 2007). PSS-coated gold nanorods can be conjugated with antibodies without any aggregation, and they are biocompatible (Caruso et al. 1997; Huang et al. 2007).

## 3.5 Toxicity of Nanoparticles and Their Clearance from the Body

It has been suggested that levels of biocompatibility and pharmacokinetics of gold nanoparticles depend strongly on their size, shape, and surface charge (Lewinski

et al. 2008; Murphy et al. 2005). In general, gold nanoparticles are much less toxic than other metal-based nanoparticles (Connor et al. 2005). One prevalent approach in testing cytotoxicity is using in vitro assays. In vitro tests of 200 mg/l gold nanospheres 24 h after administration demonstrate that the cell viability decreases by 15 % (Salem et al. 2003; Shenoy et al. 2006). Melancon et al. (2008) suggest that gold nanorods and gold nanocages are more biocompatible than gold nanoshells, since they do not contain silica. Some cytotoxic effects have been seen in gold nanoparticles smaller than 5 nm. Pan et al. (2007) reported the cytotoxicity of 1.4 nm gold nanoparticles; while 15 nm triphenylphosphine stabilized, gold particles were reported nontoxic. Also, surface charge may affect the level of toxicity of gold nanoparticles. It is reported that cationic nanoparticles are more cytotoxic than anionic nanoparticles (Goodman et al. 2004; Niidome et al. 2006; Huff et al. 2007).

Nevertheless, the production of gold nanorods requires the use of CTAB, a cationic surfactant that is also known to be a detergent suitable for degradation of biomembranes and peptides. CTAB is a stabilizing agent for nanorods (Nikoobakht and El-Sayed 2001, 2003; Niidome et al. 2006) and is evidently present after synthesis, both in the supernatant and as a bilayer on the flanks of the rods themselves. Free CTAB is certainly toxic to human cells; but it can be largely removed from preparation of gold nanorods by double centrifugal washing of the suspensions with Milli-Q™ water. The residual CTAB bilayer bound to the surface of gold nanorods is evidently not toxic to those cell types tested so far, including K562 leukemia cell line (Connor et al. 2005; Cortesi et al. 1996), RAW 264.7 murine macrophage cells (Pissuwan et al. 2007a), and the tachyzoites of the parasite *Toxoplasma gondii* (Pissuwan et al. 2007b). However, it is also demonstrated that their remaining toxicity cannot be completely neglected (Takahashi et al. 2006).

PEG, a hydrophilic polymer, has also been used to modify the surface of gold nanorods. PEG is a biocompatible polymer frequently used in drug and DNA delivery (Liu et al. 1999; Luo et al. 2002) and surface modification of gold nanorods. With a PEG coating, most in vivo and in vitro studies have indicated that gold nanoparticles have negligible toxicity, either at the cell levels or in animal experiments.

## 4 Animal and Clinical Studies of Thermal Effects of Laser Photothermal Therapy Using Gold Nanoshells/Nanorods

Despite the increasing number of publications on cancer research using laser photothermal therapy, more experimental studies are needed before laser photothermal therapy can be clinically applicable as a safe technique. Designing an optimal heating protocol to cause irreversible thermal damage to tumors relies on three major factors:

1. Heating parameters such as laser properties, selection of laser mode, duration of laser irradiance, and laser spot size

2. Gold nanorod characteristics such as gold nanorod size, gold nanorod coating, amount of gold nanorods injected, concentration of gold nanorod solutions, injection rate, number of injection sites, and injection method
3. Pre-, real-time, or post-monitoring technique to evaluate the efficacy of treatment

In this section, most recent in vitro, in vivo, and clinical studies using laser photothermal therapy are discussed and summarized.

Thermal damage to targeted tumor cells depends on temperature elevations in tumors and exposure time (Engin 1994; Welch and van Germert 1995; Dewhirst et al. 2005). For a deep-seated tumor, optical fibers may be needed to allow laser irradiation on the tumor surface. Therefore, it has been suggested that this approach not only achieves a targeted delivery of laser energy to the tumor but also maximally concentrates most of the laser energy into the tumor region. The feasibility of using gold nanoshells or nanorods to identify laser power settings for tumor destruction has been tested both in tissue culture (El-Sayed et al. 2006; Bernardi et al. 2008; Gobin et al. 2008; Melancon et al. 2008) and in implanted tumors in mice (Hirsch et al. 2003; O'Neal et al. 2004; El-Sayed et al. 2006; Stern et al. 2008; Dickerson et al. 2008; von Maltzahn et al. 2009; Manuchehrabadi et al. 2012, 2013b). A new study compares laser photothermal therapy outcome when treating human glioma spheroids with gold-silica nanoshells and gold nanorods, and they found that gold nanoshells have greater efficacy than gold nanorods (Chhetri et al. 2014).

One modification that has been suggested for improving laser photothermal therapy is the use of a pulse mode laser instead of a continuous wave (CW) laser. Pulsed lasers permit more efficient photothermal conversion because of lapses between the pulses, allowing additional time for electron-phonon relaxation. It has the potential to translate to lower power usage with a pulsed laser than with a continuous mode laser and to further minimize damage to healthy tissue. In experimental studies by Tong et al. (2007, 2009), a femtosecond-pulsed NIR laser at a power as low as 0.75 mW resulted in membrane blebs, while a continuous wave laser required a power of 6 mW for the same thermal effect.

Another important factor in successful laser photothermal therapy may be the amount of gold nanoparticles injected. The goal is to achieve desired temperature elevations with a minimal injection amount of gold nanoparticles. Thereby, the heating protocol has the benefits of cost efficiency as well as minimal toxicity. Also, based on the method of injection such as intratumoral or systemic injections, the injected volume may vary dramatically. Since most of the gold nanoparticles will be taken by the spleen and liver in a systemic delivery, more particles may be needed to achieve the same thermal dosage as in an intratumoral injection. In a new study conducted by Gao et al. (2016), transmission electron microscopy (TEM) examination revealed that silica-coated gold nanorods with high folic acid expression (GNRs@$SiO_2$-FA) entered the cells via endocytosis. This cellular uptake of gold nanorods can significantly enhance therapy outcome. Most in vivo experiments performed on mice involve injecting approximately 0.1–0.2 ml gold nanorod solution (concentration varies from $10^9$ to $10^{14}$ nanostructures per ml solution). One mouse experiment (Dickerson et al. 2008) investigated the effect of intravenous

injections versus direct injections of gold nanorods into mice bearing xenograft carcinoma to achieve the same temperature elevation (22 °C) in the tumors. 100 μl of a 120 OD gold nanorod solution was injected intravenously and was in circulation for 24 h to achieve a maximal uptake of the gold nanorods by the tumor. Then, the tumors were exposed to an 800 nm laser with an intensity of 1.7–1.9 W/cm$^2$ for 10 min. For the direct administration, mouse tumors were loaded with 15 μl of a 40 OD gold nanorod solution and irradiated with a laser radiance of 0.9–1.1 W/cm$^2$ for 2 min. Both approaches achieved similar temperature elevations in the tumors. This experiment demonstrates that more gold nanoparticles are needed in systemic delivery than in intratumoral delivery to result in the same thermal dosage in the tumor. Another study suggested that administrating nanoparticles and drug separately resulted in more than fivefold increase in intratumoral drug concentrations compared to conventional "drug-alone" administration (Colby et al. 2016). A recent study has demonstrated treatment efficacy of combining gene, drug, and gold nanorods for treating colon cancer in a mouse model (Conde et al. 2016).

Other laser parameters such as laser intensity, laser power, and laser spot size can be adjusted based on tumor location in the body, tumor size, tumor growth stage, and laser mode. Table 1 gives a summary of the laser parameters and gold nanorod characteristics for most recent photothermal therapy studies (Hirsch et al. 2003; O'Neal et al. 2004; El-Sayed et al. 2006; Dickerson et al. 2008; von Maltzahn et al. 2009; Manuchehrabadi et al. 2012). Typical laser radiance at the surface for the photothermal therapy to be effective ranges from 1 to 50 W/cm$^2$. Laser spot size, varying from 1 to 10 mm in diameter, primarily affects the tumor region laterally. Heating duration is shorter than several minutes or longer than 15 min.

Real-time monitoring of temperatures in tumors can be crucial for evaluating a designed photothermal therapy protocol. Measuring temperatures at one or two tumor locations are reported in previous studies (Hirsch et al. 2003; O'Neal et al. 2004; Melancon et al. 2008; Elliott et al. 2007; Huang et al. 2007; Dickerson et al. 2008; von Maltzahn et al. 2009; Verhaart et al. 2015; Carrasco et al. 2015). Jo et al. (2012) utilized a laser-induced fluorescence technique as a nonintrusive way to measure temperature fields around highly localized gold nanoparticle clusters. The correlation between the fluorescence intensities and temperature was investigated with two dyes by controlling the near-infrared laser intensities to heat up the particles. Schwartz et al. (2009) reported photothermal ablation via a systemic delivery of gold nanoshells to an orthotopic tumor in canine models. They compared the real-time MRI-derived temperature mappings of canine transmissible venereal tumors in the canine brain versus normal white and gray matter on the contralateral side of the brain. This study showed that laser energy of 3.5 W resulted in an average temperature of 65.8 °C in the brain exposed to heating of 3 min. Similar experiments were performed by the same group on mice, and temperature elevations were larger than 41 °C above the baseline (Stafford et al. 2011). Another group showed the feasibility of using real-time MRTI as an indirect method to estimate nanoparticle absorption (MacLellan et al. 2014). In vivo temperature mapping across human prostate cancer PC3 tumors during steady state has been reported by Manuchehrabadi et al. (2012), when the tumor surface was irradiated by a pulsed

**Table 1** Summary of laser parameters and gold nanorods characteristics for photothermal therapy applications

| Reference | Laser mode | Laser wavelength | Power intensity | Duration | Temperature elevation | GNR size | Surfactant | Injection method | Concentration | Experiment type |
|---|---|---|---|---|---|---|---|---|---|---|
| Cabada et al. (2012) | C.W. | 808 nm | 1.2 W | 1,200 s | 16 °C | 41 nm × 10 nm | CTAB | N.A. | 36 μg/mL of tissue | Cell culture astrocytoma cells |
| Lin et al. (2010) | P.W. | 810 nm | 0.5 W/cm$^2$ | 300 s | 35 °C | N.A. | CTAB | I.T. | 40 mg Au/kg | Mouse model sarcoma cells |
| | | | | | | | PEG | | | |
| Lin et al. (2012) | P.W. | 810 ± 2 nm | 1 W | 80 s | 10 °C | 42 nm × 10 nm | CTAB | N.A. | N.A. | In vitro |
| Dickerson et al. (2008) | N.A. | 800 nm | 0.9–1.1 W/cm$^2$ | 600 s | 23 °C | 50 nm × 12 nm | CTAB | I.T. | 100 μL of 40 OD | Mouse model HSC-3 cells |
| | | | | | | | PEG | | | |
| Dickerson et al. (2008) | N.A. | 800 nm | 1.7–1.9 W/cm$^2$ | 600 s | 21 °C | 50 nm × 12 nm | CTAB | I.V. | 100 μL of 120 OD | Mouse model HSC-3 cells |
| | | | | | | | PEG | | | |
| Von Maltzahn et al. (2009) | C.W. | 810 nm | 2 W/cm$^2$ | 300 s | 26 °C | 47 nm × 13 nm | CTAB | I.V. | 20 mg Au/kg | Mouse model |
| | | | | | | | PEG | | | MDA-MB-435 cells |
| Gormley et al. (2011) | P.W. | 810 nm | 1.2 W/cm$^2$ | 600 s | 10 °C | 60 nm × 15 nm | CTAB | I.V. | 9.6 mg/kg | Mouse model of sarcoma S-180 |
| | | | 1.6 W/cm$^2$ | | 7 °C | | PEG | | 120 OD | |
| Li et al. (2011) | P.W. | 810 nm | 1 W | 80 s | 10 °C | 42 nm × 10 nm | CTAB | N.A. | N.A. | Mouse model |
| El-sayed et al. (2013) | N.A. | 800 nm | 50 W/cm$^2$ | 120 s | Center 40 °C | 100 nm × 25 nm | CTAB | I.V. | 1.5 mg Au/kg | Mouse model |
| | | | | | Periphery 5 °C | | PEG | | | Ehrlich carcinoma |
| Manuchehrabadi et al. (2012) | P.W | 800 nm | 1.6 W/cm$^2$ | 600 s | 19 °C | 45 nm × 10 nm | CTAB | I.T. | 0.1 mL of 50 OD | Mouse model PC3 cells |
| | | | | | 25 °C | | PEG | | 0.1 mL of 1250OD | |

laser at 808 nm with a repetition rate of 80 MHz, resulting in a total laser energy rate at the surface as 0.6 W. The experimental results have demonstrated a temperature variation of more than 10 °C from the tumor center to its periphery, when the tumor is injected with 0.1 cc of gold nanofluid (250 OD gold nanorods). Recent parameter studies performed by Mooney et al. (2015) on a mouse model investigated the influence of combinations of nanorod concentration and laser setting on both intratumoral and tumor surface temperatures.

Temperature elevations and resulted tumor damages are dependent on all parameters discussed above. The large variations in the previous treatment protocols suggested possible variations in the tumor sizes, nanoshell/nanorod concentrations in the tumors, optical interaction with the laser light, as well as thermal effects of local blood perfusion rate in the tumors. Therefore, designing a suitable treatment protocol in laser photothermal therapy can be a very difficult and tedious task.

## 5 Monte Carlo Simulation of Laser Energy Absorption in Tissue

Methods used to simulate and analyze propagation of laser light in strongly scattering media are divided into two main types: statistical and deterministic. Deterministic methods are based on a photon transport equation and a diffuse approximation solution of a partial differential equation considering laser as a source term and the fluorescence effect of the laser beam (Anvari et al. 1994). Monte Carlo and random walks are examples of statistical methods and account for the statistic uncertainty of laser propagation in tissue (Wang et al. 1995; Flock et al. 1989). Statistical approaches require very long computation time to obtain statistically meaningful results. These methods are carried out by tracing paths of photons with simulation of scattering and absorbing patterns of light. Therefore, it is difficult to obtain solutions within practical limits of computational time when the media are large in size and complex in configuration. On the other hand, deterministic methods are based on the photon transport equation, which is in the form of an integral-differential equation, and may be difficult to solve numerically.

Wilson and Adam first introduced Monte Carlo simulations into the field of laser tissue interactions (Wilson and Adam 1983). Monte Carlo simulation is sufficiently flexible to handle complex geometrical shapes, anisotropic scattering, and non-homogeneous properties, but the results obtained by this method always have unavoidable random errors due to finite samplings. This method assumes laser as photons emitted from a laser source. Figure 1 illustrates possible path trajectories for incident photons (Manuchehrabadi et al. 2013a). After a single photon is incident on a tissue surface, the photon can either be specularly reflected or continue to transport inside the tissue. At each step the photon travels, the direction which it will be heading to, and how much energy dissipation due to absorption when the photon interacts with the tissue, is determined by probability functions. In addition, photons can interact with tissue via scattering from a particle or tiny tissue structure. During scattering, several probability functions are used to determine which direction the

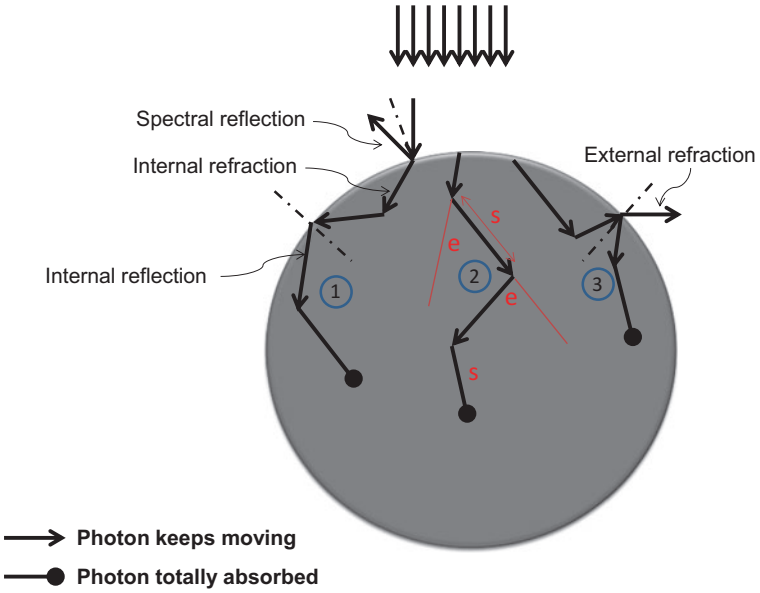


**Fig. 1** Possible path trajectories for incident photons on the top surface of a spherical tumor

photon will bend from its original path based on an anisotropic factor, as well as the length of the next step of the photon after scattering. After a series of scattering and absorption events inside the tissue, the photons may exhaust its energy to zero or escape from the tissue region. Monte Carlo simulations usually require emitting thousands of photons onto the tissue surface, based on the laser irradiation distribution. Any energy dissipation due to absorption in a unit volume element can then be added to calculate the total energy absorption rate by the element to determine the volumetric heat generation rate distribution in tissue, to be used in bioheat transfer simulation.

It is important to point out that Monte Carlo methods require previously determined radiation properties of the studied tissue, which include the absorption coefficient ($\mu_a$), the scattering coefficient ($\mu_s$), and the anisotropic factor ($g$). Optical properties of tissues are typically determined by experimental measurements of excised tissue sample (Mourant et al. 1997; MacLellan et al. 2014). For example, $\mu_s$ and $\mu_a$ of liver tissue are ten times bigger than that of prostate or breast tissue. There are several structures in the human tissues that are strong laser absorbers. Melanin in the skin and hemoglobin in the blood may greatly enhance these two coefficients (Piao et al. 2009, 2010). The anisotropic factor is nearly constant (0.9–0.97) for most tissues. An anisotropic factor close to unity implies that most scattering events result in forwarding motion of photons, rather than being scattered back to the superficial layers of tissue. One way to experimentally measure optical properties in tissue is via inverse heat

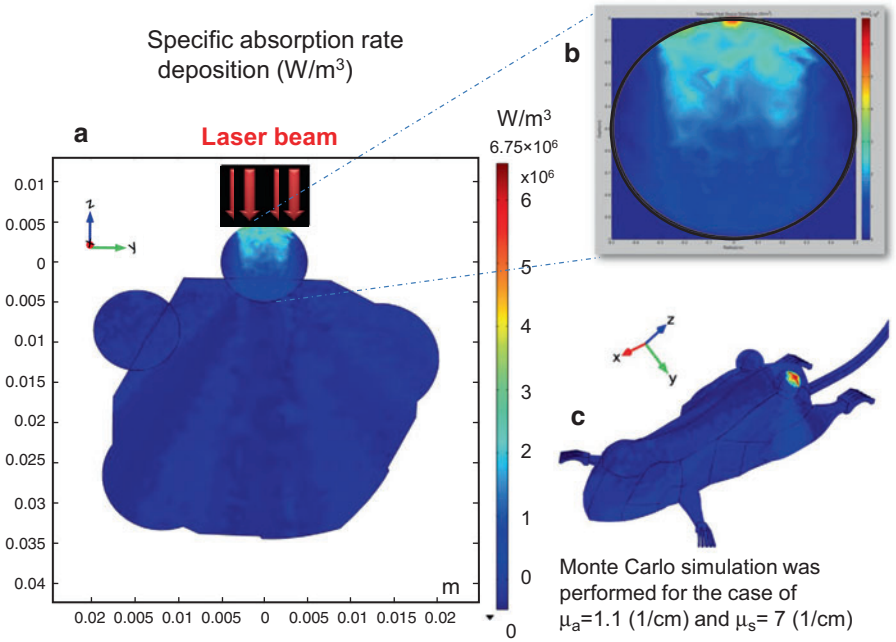


**Fig. 2** Panel (**a**) shows the SAR deposition map along the centerline in the mouse model embedded with spherical tumor. An enlarged SAR distribution is illustrated in a spherical tumor injected by 0.1 CC dosage of 250 OD concentration of gold nanorod solution (**b**). The *top* view of the SAR distribution in 3D structure of the mouse model is illustrated in panel (**c**)

transfer analyses from measured temperature distribution in tissue during heating using laser. In Manuchehrabadi et al. (2013a), a Monte Carlo model is developed to simulate laser-induced volumetric heat generation rate distribution in a spherical tumor with laser irradiance on its surface. Then, the heat generation rate source term is substituted into the Pennes bioheat equation to simulate the steady-state temperature field in the tumor during laser photothermal therapy. Both the absorption and scattering coefficients of the laser in tumors with or without gold nanorod injection are adjusted until the theoretically predicted temperature distribution agrees with that measured in their animal experiments. It has been shown that the absorption and scattering coefficients of the 808 nm laser in the tumor tissue are 1.1 $cm^{-1}$ and 7 $cm^{-1}$, respectively, when the tumor is injected with 0.1 cc of 250 OD gold nanorod solutions (Manuchehrabadi et al. 2013a). Figure 2 further illustrates the resulted volumetric heat generation rate distribution (or specific absorption rate, SAR) in the tumor using the extracted optical properties and the resulted temperature elevation in the tumor implanted in a mouse body. A major challenge of Monte Carlo simulation is how to model tumors with irregular shapes and rough surfaces; therefore, the simulation results would be more relevant to clinical/animal studies.

## 6 Modeling Heat Transfer in Biological Tissue

In biological tissues, blood flows through arteries and veins. Energy transport in biological tissues takes place through complex mechanisms of heat conduction and convection, metabolic heat generation, and heat generation from external heating sources. Many researchers have studied thermal effects of blood flow on heat transfer in living tissue and identified simplified approaches to model the thermal effects. Bioheat transfer models have been classified into two main approaches: the continuum approach and the vascular approach. Vascular approach models individual vessels as rigid tubes with blood flowing inside. Continuum models assume an average thermal effect of vasculature over a tissue domain, typically with a single global parameter to modify the traditional heat conduction equation (Bhowmik et al. 2013; Chato 1981; Charny et al. 1990). Vascular models can predict detailed information about temperature variations in both the tissue and along the blood vessels. Since animal and human vasculatures are extremely complicated, bioheat transfer modeling using vascular approach would be computationally expensive. Although vascular models are still used in applications requiring temperature distribution mapping along individual blood vessels, it is not widely used due to limitations of computational resources and lack of anatomic information of vasculatures in targeted tissue region. On the other hand, continuum models average the thermal effects of local blood perfusion to tissue, and they are relatively easy to use to predict tissue temperature distribution with reasonable accuracy (Durkee and Antich 1991).

The first continuum model was developed by Pennes (1948) to predict the energy exchange between a human forearm and its surroundings. Due to the simplicity, the Pennes bioheat equation has been implemented extensively in modeling in vivo temperature fields in tissue in therapeutic hyperthermia (El-dabe et al. 2003; Nield and Kuznetsov 2009; Raaymakers et al. 2009; Minkowycz et al. 2012; Rodrigues et al. 2013; Li et al. 2013). The Pennes bioheat equation neglects all pre-arteriole and post-venule heat transfer between blood and tissue and the effect of blood flow directionality. Also in this model, it is assumed that blood instantaneously exchanges energy and equilibrates with the local tissue temperature, with the arterioles supplying the capillary beds at the body core temperature. Therefore, the thermal effect of local blood perfusion is modeled as an isotropic, however, nonuniform heat source, or sink distribution.

Pennes formulated his classic bioheat equation (Pennes 1948) as

$$\rho c \frac{\partial T}{\partial t} = \nabla \bullet (k \nabla T) + \omega \rho_b c_b (T_b - T) + q_m + Q \tag{1}$$

where subscript $b$ refers to blood. Local blood perfusion rate is designated as$\omega$. $T$ is tissue temperature, $k$ is tissue thermal conductivity, $\rho$ is density, $c$ is specific heat, $T_b$ is the arterial temperature and is often assumed to be equal to the body core temperature, $q_m$ is the volumetric heat generation rate due to metabolism, and $Q$ is the volumetric heat generation rate generated by external heating devices. The blood perfusion term in the Pennes bioheat equation is a key factor to the temperature

gradients within the tissue in clinical applications, and it is assumed to be proportional to the local blood perfusion rate and the temperature difference between blood and tissue (Kreith 2000). Good agreements between model predictions and experimental results can be found if the local blood perfusion rate is considered as an adjustable parameter. The limitation of the Pennes bioheat equation is due to its neglecting venous rewarming that may play an important role in countercurrent heat exchange.

Considerable modifications have been proposed by various researchers to address the limitations of the Pennes bioheat equation. In order to take into consideration of blood flow directions, Wulff and Klinger (Wulff 1974) considered the local blood mass flux. Chen and Holmes (1980) have studied the effect of thermal equilibration length on the blood temperature. They modified the Klinger equation by adding dispersion and microcirculatory perfusion terms (Vafai 2015). In 1984, Jiji et al. (1984) presented a new continuum bioheat model by considering the countercurrent heat exchange between artery and vein as the dominate heat transfer mechanism in bioheat transfer. The Weinbaum-Jiji model implies a substantial temperature difference between the tissue and the venous blood and emphasizes rewarming in the venous blood by its countercurrent arterial blood. In the Weinbaum-Jiji model, the contribution of local blood flow is expressed by an enhancement in thermal conductivity of the tissue in the heat conduction equation:

$$\rho c \frac{\partial T}{\partial t} = \nabla \bullet (k_{\text{eff}} \nabla T) + q_m + Q \tag{2}$$

where $k_{\text{eff}} = k(1 + f(\omega))$, the effective thermal conductivity due to countercurrent artery and vessel pairs, and $f(\omega)$ accounts for the geometric properties of the blood vessels, their number density and the blood velocity. Due to the difficulty of implementation and determination of the exact expression to calculate the enhancement in thermal conductivity, the Weinbaum-Jiji bioheat equation never reached the popularity of the Pennes bioheat equation in bioheat modeling applications.

## 7 Assessment of Thermal Damage

An optimal heating protocol for a heating experiment can be determined based on the Arrhenius integral or the $EM_{43}$, an alternative parameter derived from the Arrhenius integral (Moritz and Henriques 1947; Sapareto and Dewey 1984; Dewhirst et al. 2003; Diederich 2005). The Arrhenius integral (Moritz and Henriques 1947) can be used to quantitatively assess thermal damage based on measured or simulated temperature history at various tissue locations. Damage is considered to be a unimolecular process. In this process, the native molecules are transformed into a coagulated state, leading to cell death. Damage is quantified as a single dimensionless parameter $\Omega$ (Qin et al. 2014). This equation is referred to as the Arrhenius integral as follows:

$$\Omega(x,y,z,r) = \ln\left[\frac{C(0)}{C(\tau)}\right] = F\int_0^{\tau} e^{-\frac{E_a}{R_u T(x,y,z,t)}}\mathrm{dt} \tag{3}$$

where $t$ is time, $C$ is the concentration of undamaged cells, $F$ is the pre-exponential factor or frequency factor (1/s), $E_a$ is the activation energy barrier (J/mole), $R_u$ is the universal gas constant (J/mole.K), and $T(x,y,z,t)$ is the absolute tissue temperature at the location $(x,y,z)$. $\Omega$, the extent of damage, is defined as the logarithm of the ratio of the initial concentration of the healthy cells, $C(0)$, to the concentration of the healthy cells remaining after thermal treatment, $C(\tau)$, for a duration of $\tau$. The value of $\Omega$ is zero before any thermal therapy, and it increases during heating. 63% and 98.2% denaturation of protein occurs when $\Omega = 1$ and 4, respectively (Chang and Nguyen 2004). Note that $\Omega$ is a function of both tissue location $(x,y,z)$ and heating time $\tau$. Implementing the integral requires knowing the activation energy and the frequency factor associated with the tissue cells. The values of $E_a$ and $F$ are determined by inverse thermal analyses in matching the model to the data for cell injury and temperature-time history of exposure. The activation energy and frequency factor are related to activation enthalpy and entropy. From the exponential nature of the equation, it suggests that rate damage accumulation will be negligible below certain temperature threshold. Once the threshold value is exceeded, a swift increase in the rate damage accumulation is expected.

This approach has been used to design a treatment protocol in laser photothermal therapy (Manuchehrabadi and Zhu 2014). Figure 3 illustrates the approach of using laser photothermal therapy in treating a prostatic tumor. The design procedures rely on simultaneous simulations of the laser energy absorption (Monte Carlo), temperature distribution in the tumor (Pennes bioheat equation), and thermal damage

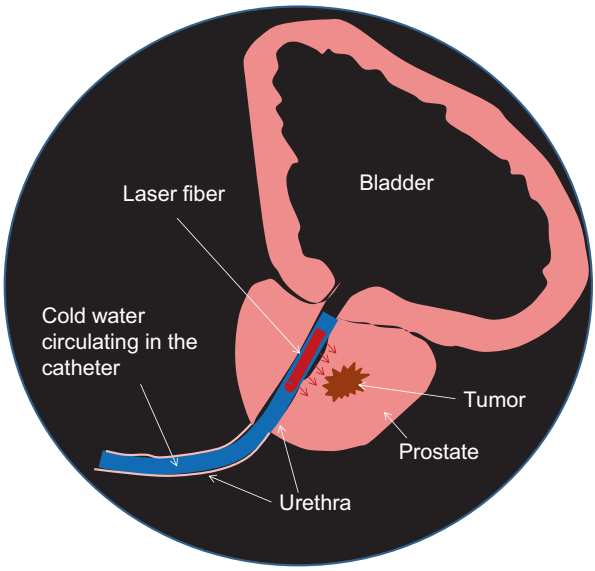


**Fig. 3** Schematic diagram of laser photothermal therapy in treating prostatic cancer. A catheter with an embedded laser fiber is inserted through the prostatic urethra, supported by cooling water circulating inside the catheter to protect the urethra from overheating. Laser energy is emitted from the laser fiber to reach the tumor

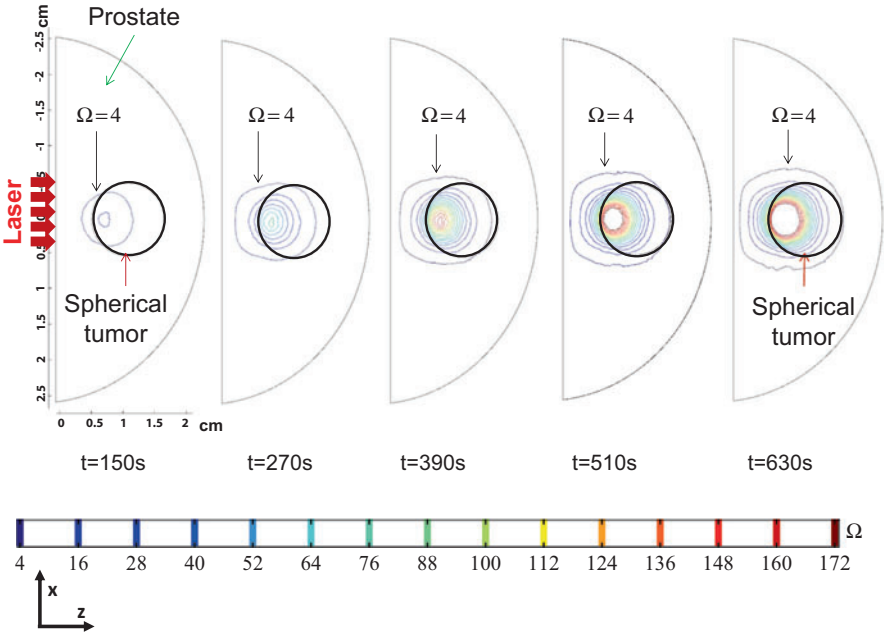


**Fig. 4** Coronal views of thermal damage contours ($\Omega = 4$) at different time instants, when the blood perfusion rate is assumed to be temperature dependent

assessment (Arrhenius integral). The blood perfusion rate in the tumor is considered tissue temperature dependent. The parameters in the Arrhenius integral are modeled as dependent on both the tissue type and local temperature. Figure 4 depicts the thermal damage contour evolution during the heating. Note that the laser is irradiated on the urethral surface, and laser energy penetrates the prostatic tissue to reach the spherical tumor. After laser heating of 153 s, the thermally damaged tumor region ($\Omega \geq 4$) only covers one-third of the entire tumor. After about 630 s (10.5 min) of heating, 100 % of the tumor is damaged. Extensive thermal injury also occurs in the healthy tissue region between the urethra and the top surface of the tumor; however, the collateral damage region percentage is lower than a threshold of 5 %. Therefore, the designed heating protocol to treat a 10 mm diameter tumor in the human prostate is determined as a heating duration of 10.5 min, assuming one uses the laser parameter setting in the model.

The major challenge is that the magnitudes of the coefficients are cell dependent. It is important to relate the results from the thermal damage model to pathological end points such as collagen damage, thermal coagulation, reversible cell injury, etc. It has also been found that heat tolerance varies from one kind of tumors to another, and heating time at certain temperatures strongly depends on cancer type and growth stage. One previous experimental study of thermal tolerance of various carcinoma cells has demonstrated that human prostatic carcinoma cell lines are much easier to

be damaged than carcinoma cell lines of other human origin, such as the colon, breast, lung, and brain, under the same mild hyperthermia dosage (Ryu et al. 1996).

In clinical studies of specific cancer type and growth stage, it is a common practice to perform experiments at 43 °C to determine how long it takes to induce certain thermal damage (edema, necrosis, etc.), and this time duration is called $EM_{43}$. The $EM_{43}$, the thermal isoeffective dose, converts the temperature levels and heating duration into an equivalent number of minutes at 43 °C to induce thermal damage to a specific tumor cell type (Sapareto and Dewey 1984; Diederich 2005; Pearce 2009; Qin et al. 2014). A summary by Dewhirst et al. (2003) shows a wide range of $EM_{43}$values for various tissue types, suggesting complicated biological and chemical factors that may contribute to the wide variation in estimating the threshold of thermal damage. Cumulative equivalent minutes from any heating experiments can then be calculated and compared to $EM_{43}$ of the same tumor cell line. $EM_{43}$ is proposed to be estimated by the following equation (Dewhirst et al. 2003):

$$\mathrm{EM}_{43} = \sum_i \Delta t_i R^{(43-T_i)}$$

$$R = \begin{cases} 0.25 & 37^{\circ}\mathrm{C} \le \mathrm{T} \le 43^{\circ}\mathrm{C} \\ 0.50 & 43^{\circ}\mathrm{C} \le \mathrm{T} < \ < 48^{\circ}\mathrm{C} \\ 0.72 & 48^{\circ}\mathrm{C} \le \mathrm{T} \end{cases} \tag{4}$$

where $T_i$ is measured or predicted temperatures in Celsius at certain tissue locations and $\Delta t_i$ is the time duration at temperature $T_i$. When the tissue temperature is higher than 43 °C, the equivalent minutes at 43 °C is longer than the actual heating time. For example, if the temperature is maintained at 45 °C for 5 min, i.e.,= 5 min, the equivalent minutes for this time segment (20 min) will be longer than 5 min with an $R$-value of 0.5. In another word, the equivalent minutes can be much higher than the actual heating time when the tumor temperature is higher than 43 °C. If the calculated number of the equivalent minutes of a heating protocol is longer than the $EM_{43}$ of the same tumor cell line, irreversible thermal damage is ensured. Since $EM_{43}$ depends on the measured or predicted temperature elevation history, it may vary from one tumor location from another. Therefore, estimating $EM_{43}$ over the entire tumor can provide assessment of a thermal damage region within the tumor and its surrounding tissue. If the temperature field is predicted via theoretical simulation, the heating protocol can be modified to achieve the objective to have the thermal damage region covering the entire tumor and to have minimal damage occurring to the surrounding healthy tissue. A recent study by Manuchehrabadi et al. (2013b) has used the approach to estimate the $EM_{43}$ in PC3 tumors implanted in mice. The heating is induced by an 808 nm laser with a heating duration of 15 min. Based on the measured temperature mapping along two tumor paths in an in vivo experiment, one estimates the $EM_{43}$values at all the measurement locations. More than 93% of the locations have an $EM_{43}$ value longer than 110 min. Later the results are compared to histological analyses and tumor shrinkage studies after the same

treatment protocol. The distribution of thermal damage observed in the experiment agrees with the theoretical prediction of the $EM_{43}$ values.

Previous studies have demonstrated complicated biological and chemical factors that may contribute to the wide range of the threshold thermal dosage. It strongly suggests that experimental studies are necessary to evaluate thermal damage to tumors to extract either the coefficients used in the Arrhenius integral or the $EM_{43}$ value, to assess whether a future treatment protocol is likely to induce adequate thermal damage to targeted tumor cells.

## 8 Conclusion Remarks

While hyperthermia therapies using microwave, RF, and ultrasound are commercially available and have been used in some clinical studies, gold nanorod-/nanoshell-based laser photothermal therapy is not a standard treatment for cancer patients, despite its great potential and numerous advantages. A number of challenges need to be addressed before it reaches the level of first-line clinical studies.

In most of the current studies, gold nanorods/nanoshells are delivered via a single intratumoral injection to tumors embedded on the superficial area of the flank of the mice. It is not clear whether the obtained distribution of gold nanoparticles in one kind of tumors can be applied to other types of tumors. Based on current understanding, microstructural transport properties of tumors may be different from one type of tumors to another, and it may also be affected by tumor growth stages. For example, it is speculated that human prostate cancer PC4 tumors are much denser than human prostate cancer PC3 tumors; therefore, the resulted nanoparticle deposition patterns may be different. Further, if the gold nanoparticle distribution is not uniform, it will add complexity in Monte Carlo methods to simulate photon propagation in a tissue domain with nonuniform optical properties of the laser.

When a tumor is located in a superficial region with easy access by needle, intratumoral injections can be utilized to deliver gold nanoparticle solutions. For deep-seated tumors, one challenge could be the difficulty of intratumoral administration of gold nanoparticles. It is possible that intravenous delivery may be the only option. It is not clear how injection parameters in intravenous infusion would affect the resulted nanoparticle deposition in tumors. More studies are needed to investigate how to modify nanoparticle surface coating to enhance the number of nanoparticles trapped by targeted tumors. In addition, after nanoparticle delivery, it is still a challenge to deliver laser to tumors with minimal laser energy wasted in healthy tissue.

Since ultimate thermal damage depends on temperature elevation history and heating duration, it is important to evaluate simultaneously both temperature elevations and treatment efficacy (histological analyses and tumor shrinkages). One improvement to the current studies includes minimally noninvasive temperature mapping in the entire tumor during in vivo laser treatment. Thermocouples can be used to provide temperature information at limited locations in tumors. Other

methods such as 3-D MRI may be a feasible approach to map the 3-D temperature distribution if it does not interfere with laser delivery.

Another future improvement is in the Monte Carlo simulation that is typically conducted in geometries with regular shapes. Since human tumors may have different shapes and sizes, it will be very helpful to perform Monte Carlo simulation on a tumor geometry based on MRI or CT scans of the specific tumor. It is difficult to achieve individualized heating protocol design without considering patient-specific tumor sizes and shapes. In addition, the location of the tumor in the organ relative to the laser irradiation surface is also a very important factor that may affect the thermal dosage deposited in tumors.

To design a treatment protocol for individual tumors using theoretical simulation required extensive parametrical studies to identify dominant factors that will greatly influence the resulted thermal dosage. In addition to modeling the precise shape and size of tumors, important parameters may be the optical properties of the laser in the targeted tumor. Unfortunately, there is very limited information on the properties. More experimental studies are needed to directly measure those properties or to extract the properties based on inverse heat transfer analyses. Further, there have been quite a lot of studies recently focused on developing alternative thermal damage assessment models, reflecting the observed discrepancy between theoretical and experimental results. For example, a recent study by Pearce (2015) has proposed a modified Arrhenius model adding a "shoulder" region before the typical linear curve. It has been shown that agreement between experimental measurements of cell death and prediction by the Arrhenius model is improved significantly once a temperature-dependent time delay ("shoulder") is implemented. Future experimental studies should be designed to examine its effect on the thermal dosage and treatment efficacy. Strong collaboration between engineers and clinicians is also necessary to develop experimental approach to validate designed treatment protocols. This includes quantitative histological analyses and long-term follow-up of tumor shrinkage after the heating treatment. In addition, histological analyses and tumor shrinkage studies can be coupled with dynamic markers such as release of heat shock proteins (HSP), a critical component of cellular defense mechanism under adverse environmental conditions. Characterization of thermally induced HSP kinetics can be helpful for designing protocols during laser therapy by controlling the tissue response to therapy based on accurate prediction of the HSP expression and damage distributions.

**Acknowledgment** This work was supported by an NSF grant (CBET-1335958).

## 9 Cross-References

► Heat Transfer In Vivo: Phenomena and Models
► Heat Transfer Physics: From Nano- to Macro-scales
► Monte Carlo Methods for Radiative Transfer

## References

Aaseth J, Haugen M, Forre O (1998) Rheumatoid arthritis and metal compounds–perspectives on the role of oxygen radical detoxification. Analyst 123(1):3–6

American Cancer Society (2016) Cancer facts and figures. American Cancer Society, Atlanta

Amreddy N, Muralidharan R, Babu A, Mehta M, Johnson EV, Zhao YD, Munshi A, Ramesh R (2015) Tumor-targeted and pH-controlled delivery of doxorubicin using gold nanorods for lung cancer therapy. Int J Nanomedicine 10:6773

Anvari B, Rastegar S, Motamedi M (1994) Modeling of intraluminal heating of biological tissue: implications for treatment of benign prostatic hyperplasia. IEEE Trans Biomed Eng 41 (9):854–864

Ashokkumar T, Prabhu D, Geetha R, Govindaraju K, Manikandan R, Arulvasu C, Singaravelu G (2014) Apoptosis in liver cancer (HepG2) cells induced by functionalized gold nanoparticles. Colloids Surf B: Biointerfaces 123:549–556

Bazile D, Prud'homme C, Bassoullet M-T, Marlard M, Spenlehauer G, Veillard M (1995) Stealth Me. PEG-PLA nanoparticles avoid uptake by the mononuclear phagocytes system. J Pharm Sci 84(4):493–498

Berlien HMG (2003) Applied laser medicine. Springer, Berlin

Bernardi RJ, Lowery AR, Thompson PA, Blaney SM, West JL (2008) Immunonanoshells for targeted photothermal ablation in medulloblastoma and glioma: an in vitro evaluation using human cell lines. J Neuro-Oncol 86(2):165–172

Berry V, Gole A, Kundu S, Murphy CJ, Saraf RF (2005) Deposition of CTAB-terminated nanorods on bacteria to form highly conducting hybrid systems. J Am Chem Soc 127 (50):17600–17601

Bhowmik A, Singh R, Repaka R, Mishra SC (2013) Conventional and newly developed bioheat transport models in vascularized tissues: a review. J Therm Biol 38(3):107–125

Black KC, Kirkpatrick ND, Troutman TS, Xu L, Vagner J, Gillies RJ, Barton JK, Utzinger U, Romanowski M (2008) Gold nanorods targeted to delta opioid receptor: plasmon-resonant contrast and photothermal agents. Mol Imaging 7(1):50–57

Boris K, Vladimir Z, Andrei M, Valery T, Nikolai K (2006) Optical amplification of photothermal therapy with gold nanoparticles and nanoclusters. Nanotechnology 17(20):5167

Bush W (1886) Uber den finfluss wetchen heftigere eryspelen zuweilen auf organlsierte neubildungen dusuben. Verh Natruch Peuss Rhein Westphal 23:28–30

Cabada TF, de Pablo CS, Serrano AM, del Pozo Guerrero F, Olmedo JJ, Gomez MR (2012) Induction of cell death in a glioblastoma line by hyperthermic therapy based on gold nanorods. Int J Nanomed 7:1511

Cai W, Gao T, Hong H, Sun J (2008) Applications of gold nanoparticles in cancer nanotechnology. Nanotechnol Sci Appl. doi:10.2147/NSA.S37888

Carrasco E, del Rosal B, Sanz-Rodríguez F, de la Fuente ÁJ, Gonzalez PH, Rocha U, Kumar KU, Jacinto C, Solé JG, Jaque D (2015) Intratumoral thermal reading during photo-thermal therapy by multifunctional fluorescent nanoparticles. Adv Funct Mater 25(4):615–626

Caruso F, Niikura K, Furlong DN, Okahata Y (1997) 2. Assembly of alternating polyelectrolyte and protein multilayer films for immunosensing. Langmuir 13(13):3427–3433

Chang IA, Nguyen UD (2004) Thermal modeling of lesion growth with radiofrequency ablation devices. Biomed Eng Online 3(1):1

Charny CK, Weinbaum S, Levin RL (1990) An evaluation of the Weinbaum-Jiji bioheat equation for normal and hyperthermic conditions. J Biomech Eng 112(1):80–87

Chato JC (1981) ASME centennial historical perspective paper: reflections on the history of heat and mass transfer in bioengineering. J Biomech Eng 103(2):97–101

Chaussy C, Thüroff S (2004) Results and side effects of high-intensity focused ultrasound in localized prostate cancer. J Endourol 15(4):437–440

Cheheltani R, Ezzibdeh RM, Chhour P, Pulaparthi K, Kim J, Jurcova M, Hsu JC, Blundell C, Litt HI, Ferrari VA, Allcock HR, Sehgal CM, Cormode DP (2016) Tunable, biodegradable gold

nanoparticles as contrast agents for computed tomography and photoacoustic imaging. Biomaterials 102:87–97
Chen MM, Holmes KR (1980) Microvascular contributions in tissue heat transfer. Ann N Y Acad Sci 335(1):137–150
Chen Q, Li K, Wen S, Liu H, Peng C, Cai H, Shen M, Zhang G, Shi X (2013) Targeted CT/MR dual mode imaging of tumors using multifunctional dendrimer-entrapped gold nanoparticles. Biomaterials 34(21):5200–5209
Cherukuri P, Glazer ES, Curley SA (2010) Targeted hyperthermia using metal nanoparticles. Adv Drug Deliv Rev 62(3):339–345
Chhetri S, Hirschberg H, Madsen SJ (2014) Photothermal therapy of human glioma spheroids with gold-silica nanoshells and gold nanorods: a comparative study. In: Proceedings of SPIE 8928, optical techniques in neurosurgery, neurophotonics, and optogenetics, 89280U
Choi M-R, Stanton-Maxey KJ, Stanley JK, Levin CS, Bardhan R, Akin D, Badve S, Sturgis J, Robinson JP, Bashir R, Halas NJ, Clare SE (2007) A cellular trojan horse for delivery of therapeutic nanoparticles into tumors. Nano Lett 7(12):3759–3765
Chon JWM, Bullen C, Zijlstra P, Gu M (2007) Spectral encoding on gold nanorods doped in a silica sol–gel matrix and its application to high-density optical data storage. Adv Funct Mater 17 (6):875–880
Colby AH, Liu R, Schulz MD, Padera RF, Colson YL, Grinstaff MW (2016) Two-step delivery: exploiting the partition coefficient concept to increase intratumoral paclitaxel concentrations in vivo using responsive nanoparticles. Sci Rep 6:18720
Cole JR, Mirin NA, Knight MW, Goodrich GP, Halas NJ (2009) Photothermal efficiencies of nanoshells and nanorods for clinical therapeutic applications. J Phys Chem C 113 (28):12090–12094
Conde J, Oliva N, Zhang Y, Artzi N (2016) Local triple-combination therapy results in tumour regression and prevents recurrence in a colon cancer model. Nat Mater 15:1128–1138. advance online publication
Connor EE, Mwamuka J, Gole A, Murphy CJ, Wyatt MD (2005) Gold nanoparticles are taken up by human cells but do not cause acute cytotoxicity. Small 1(3):325–327
Cortesi R, Esposito E, Menegatti E, Gambari R, Nastruzzi C (1996) Effect of cationic liposome composition on in vitro cytotoxicity and protective effect on carried DNA. Int J Pharm 139(1):69–78
Decuzzi P, Pasqualini R, Arap W, Ferrari M (2008) Intravascular delivery of particulate systems: does geometry really matter? Pharm Res 26(1):235–243
Dewhirst M, Viglianti B, Lora-Michiels M, Hanson M, Hoopes P (2003) Basic principles of thermal dosimetry and thermal thresholds for tissue damage from hyperthermia. Int J Hyperth 19 (3):267–294
Dewhirst MW, Vujaskovic Z, Jones E, Thrall D (2005) Re-setting the biologic rationale for thermal therapy. Int J Hyperth 21(8):779–790
Dickerson EB, Dreaden EC, Huang X, El-Sayed IH, Chu H, Pushpanketh S, McDonald JF, El-Sayed MA (2008) Gold nanorod assisted near-infrared plasmonic photothermal therapy (PPTT) of squamous cell carcinoma in mice. Cancer Lett 269(1):57–66
Diederich CJ (2005) Thermal ablation and high-temperature thermal therapy: overview of technology and clinical implementation. Int J Hyperth 21(8):745–753
Durkee J Jr, Antich P (1991) Exact solutions to the multi-region time-dependent bioheat equation with transient heat sources and boundary conditions. Phys Med Biol 36(3):345
Durr NJ, Larson T, Smith DK, Korgel BA, Sokolov K, Ben-Yakar A (2007) Two-photon luminescence imaging of cancer cells using molecularly targeted gold nanorods. Nano Lett 7 (4):941–945. doi:10.1021/nl062962v
El-dabe NTM, Mohamed M, El-Sayed AF (2003) Effects of microwave heating on the thermal states of biological tissues. Afr J Biotechnol 2(11):453–459
Elliott AM, Stafford RJ, Schwartz J, Wang J, Shetty AM, Bourgoyne C, O'Neal P, Hazle JD (2007) Laser-induced thermal response and characterization of nanoparticles for cancer treatment using magnetic resonance thermal imaging. Med Phys 34(7):3102–3108

El-Sayed MA, Shabaka AA, El-Shabrawy OA, Yassin NA, Mahmoud SS, El-Shenawy SM, Al-Ashqar E, Eisa WH, Farag NM, El-Shaer MA, Salah N (2013) Tissue distribution and efficacy of gold nanorods coupled with laser induced photoplasmonic therapy in ehrlich carcinoma solid tumor model. PLoS One 8(10):e76207

El-Sayed IH, Huang X, El-Sayed MA (2006) Selective laser photo-thermal therapy of epithelial carcinoma using anti-EGFR antibody conjugated gold nanoparticles. Cancer Lett 239 (1):129–135. doi:10.1016/j.canlet.2005.07.035

Engin K (1994) Biological rationale for hyperthermia in cancer treatment (II). Neoplasma 41 (5):277–283

Flock ST, Patterson MS, Wilson BC, Wyman DR (1989) Monte Carlo modeling of light propagation in highly scattering tissues. I. Model predictions and comparison with diffusion theory. IEEE Trans Biomed Eng 36(12):1162–1168

Gao B, Xu J, He K-W, Shen L, Chen H, Yang H-J, Li A-H, Xiao W-H (2016) Cellular uptake and intra-organ biodistribution of functionalized silica-coated gold nanorods. Mol Imaging Biol 18:1–10

Garg S, Vermani K, Garg A, Anderson AR, Rencher BW, Zaneveld DLJ (2005) Development and characterization of bioadhesive vaginal films of sodium polystyrene sulfonate (PSS), a novel contraceptive antimicrobial agent. Pharm Res 22(4):584–595

Gelet A, Chapelon JY, Bouvier R, Rouviere O, Lasne Y, Lyonnet D, Dubernard JM (2000) Transrectal high-intensity focused ultrasound: minimally invasive therapy of localized prostate cancer. J Endourol/Endourol Soc 14(6):519–528

Gobin AM, Moon JJ, West JL (2008) EphrinA I-targeted nanoshells for photothermal ablation of prostate cancer cells. Int J Nanomedicine 3(3):351–358

Gong T, Olivo M, Dinish US, Goh D, Kong KV, Yong K-T (2013) Engineering bioconjugated gold nanospheres and gold nanorods as label-free plasmon scattering probes for ultrasensitive multiplex dark-field imaging of cancer cells. J Biomed Nanotechnol 9(6):985–991

Goodman CM, McCusker CD, Yilmaz T, Rotello VM (2004) Toxicity of gold nanoparticles functionalized with cationic and anionic side chains. Bioconjug Chem 15(4):897–900

Gorelikov I, Field LM, Kumacheva E (2004) Hybrid microgels photoresponsive in the near-infrared spectral range. J Am Chem Soc 126(49):15938–15939

Gormley AJ, Greish K, Ray A, Robinson R, Gustafson JA, Ghandehari H (2011) Gold nanorod mediated plasmonic photothermal therapy: a tool to enhance macromolecular delivery. Int J Pharma 415(1):315–318

Guo Z, Fan X, Liu L, Bian Z, Gu C, Zhang Y, Gu N, Yang D, Zhang J (2010) Achieving high-purity colloidal gold nanoprisms and their application as biosensing platforms. J Colloid Interface Sci 348(1):29–36

Harris JM, Chess RB (2003) Effect of pegylation on pharmaceuticals. Nat Rev Drug Discov 2 (3):214–221

Heilmann A, Kreibig U (2000) Optical properties of embedded metal nanoparticles at low temperatures. Eur Phys J Appl Phys 10(3):193–202

Hirsch LR, Stafford RJ, Bankson JA, Sershen SR, Rivera B, Price RE, Hazle JD, Halas NJ, West JL (2003) Nanoshell-mediated near-infrared thermal therapy of tumors under magnetic resonance guidance. Proc Natl Acad Sci USA 100(23):13549–13554

Huang X, El-Sayed IH, Qian W, El-Sayed MA (2006) Cancer cell imaging and photothermal therapy in the near-infrared region by using gold nanorods. J Am Chem Soc 128(6):2115–2120

Huang X, Jain PK, El-Sayed IH, El-Sayed MA (2007) Plasmonic photothermal therapy (PPTT) using gold nanoparticles. Lasers Med Sci 23(3):217–228

Huang X, Jiang P, Tanaka T (2011) A review of dielectric polymer composites with high thermal conductivity. IEEE Electr Insul Mag 27(4):8–16

Huff TB, Hansen MN, Zhao Y, Cheng JX, Wei A (2007) Controlling the cellular uptake of gold nanorods. Langmuir 23(4):1596–1599. doi:10.1021/la062642r

Issels RD, Lindner LH, Verweij J, Wust P, Reichardt P, Schem B-C, Abdel-Rahman S, Daugaard S, Salat C, Wendtner C-M, Vujaskovic Z, Wessalowski R, Jauch K-W, Dürr HR, Ploner F, Baur-

Melnyk A, Mansmann U, Hiddemann W, Blay J-Y, Hohenberger P (2010) Neo-adjuvant chemotherapy alone or with regional hyperthermia for localised high-risk soft-tissue sarcoma: a randomised phase 3 multicentre study. Lancet Oncol 11(6):561–570

Jain PK, Lee KS, El-Sayed IH, El-Sayed MA (2006) Calculated absorption and scattering properties of gold nanoparticles of different size, shape, and composition: applications in biological imaging and biomedicine. J Phys Chem B 110(14):7238–7248

Jain S, Hirst DG, O'Sullivan JM (2012) Gold nanoparticles as novel agents for cancer therapy. Br J Radiol 85(1010):101–113

Jana NR, Gearheart L, Murphy CJ (2001) Wet chemical synthesis of high aspect ratio cylindrical gold nanorods. J Phys Chem B 105(19):4065–4067

Jiji LM, Weinbaum S, Lemons DE (1984) Theory and experiment for the effect of vascular microstructure on surface tissue heat transfer – part II: model formulation and solution. J Biomech Eng 106(4):331–341

Jo W, Lee JH, Kim MJ (2012) Temperature measurement in a single patterned gold nanorod cluster using laser-induced fluorescence. J Nanopart Res 14(1):1–11

Johannsen M, Gneveckow U, Eckelt L, Feussner A, WaldÖFner N, Scholz R, Deger S, Wust P, Loening SA, Jordan A (2005) Clinical hyperthermia of prostate cancer using magnetic nanoparticles: presentation of a new interstitial technique. Int J Hyperth 21(7):637–647

Joshi P, Chakraborti S, Ramirez-Vick JE, Ansari ZA, Shanker V, Chakrabarti P, Singh SP (2012) The anticancer activity of chloroquine-gold nanoparticles against MCF-7 breast cancer cells. Colloids Surf B: Biointerfaces 95:195–200

Kang Y, Taton TA (2005) Controlling shell thickness in core−shell gold nanoparticles via surface-templated adsorption of block copolymer surfactants. Macromolecules 38(14):6115–6121

Katz E, Willner I (2004) Integrated nanoparticle–biomolecule hybrid systems: synthesis, properties, and applications. Angew Chem Int Ed 43(45):6042–6108

Kennedy LC, Bickford LR, Lewinski NA, Coughlin AJ, Hu Y, Day ES, West JL, Drezek RA (2011) A new era for cancer treatment: gold-nanoparticle-mediated thermal therapies. Small 7 (2):169–183

Kim F, Song JH, Yang P (2002) Photochemical synthesis of gold nanorods. J Am Chem Soc 124 (48):14316–14317

Kim B, Han G, Toley BJ, Kim CK, Rotello VM, Forbes NS (2010) Tuning payload delivery in tumour cylindroids using gold nanoparticles. Nat Nanotechnol 5(6):465–472

Kogan B, Andronova N, Khlebtsov N, Khlebtsov B, Rudoy V, Dement'eva O, Sedykh E, Bannykh L (2008) Pharmacokinetic study of PEGylated plasmon resonant gold nanoparticles in tumor-bearing mice. Tech Proc 2008 NSTI Nanotechnol Conf 2:65–68

Krag DN, Fuller SP, Oligino L, Pero SC, Weaver DL, Soden AL, Hebert C, Mills S, Liu C, Peterson D (2002) Phage-displayed random peptide libraries in mice: toxicity after serial panning. Cancer Chemother Pharmacol 50(4):325–332

Kreith F (2000) Handbook of thermal engineering. CRC Press, Boca Raton

Lal S, Clare SE, Halas NJ (2008) Nanoshell-enabled photothermal cancer therapy: impending clinical impact. Acc Chem Res 41(12):1842–1851

Lanuti M, Sharma A, Digumarthy SR, Wright CD, Donahue DM, Wain JC, Mathisen DJ, Shepard J-AO (2009) Radiofrequency ablation for treatment of medically inoperable stage I non–small cell lung cancer. J Thorac Cardiovasc Surg 137(1):160–166

Larson TR, Blute ML, Bruskewitz RC, Mayer RD, Ugarte RR, Utz WJ (1998) A high-efficiency microwave thermoablation system for the treatment of benign prostatic hyperplasia: results of a randomized, sham-controlled, prospective, double-blind, multicenter clinical trial. Urology 51 (5):731–742

Lewinski N, Colvin V, Drezek R (2008) Cytotoxicity of nanoparticles. Small 4(1):26–49

Li Z, Jin R, Mirkin CA, Letsinger RL (2002) Multiple thiol-anchor capped DNA–gold nanoparticle conjugates. Nucleic Acids Res 30(7):1558–1562

Li FM, Liu JM, Wang XX, Lin LP, Cai WL, Lin X, Zeng YN, Li ZM, Lin SQ (2011) Non-aggregation based label free colorimetric sensor for the detection of Cr (VI) based on selective etching of gold nanorods. Sens Actuat B Chem 155(2):817–822

Li J, Gupta S, Li C (2013) Gold nanoparticles in cancer theranostics. Quant Imaging Med Surg 3(6):284–291

Liang Z, Susha A, Caruso F (2003) Gold nanoparticle-based core−shell and hollow spheres and ordered assemblies. There Chem Mater 15(16):3176–3183

Lin HW, Lu YJ, Chen HY, Lee HM, Gwo S, (2010) InGaN/GaN nanorod array white light-emitting diode. Appl Phys Lett 97(7):073101

Lin YG, Hsu YK, Chen YC, Wang SB, Miller JT, Chen LC, Chen KH (2012) Plasmonic Ag@ Ag 3 (PO 4) 1−x nanoparticle photosensitized ZnO nanorod-array photoanodes for water oxidation. Energy Environ Sci 5(10):8917–22

Link S, El-Sayed MA (1999) Spectral properties and relaxation dynamics of surface plasmon electronic oscillations in gold and silver nanodots and nanorods. J Phys Chem B 103 (40):8410–8426

Link S, El-Sayed MA (2000) Shape and size dependence of radiative, non-radiative and photo-thermal properties of gold nanocrystals. Int Rev Phys Chem 19(3):409–453

Link S, Mohamed MB, El-Sayed MA (1999) Simulation of the optical absorption spectra of gold nanorods as a function of their aspect ratio and the effect of the medium dielectric constant. J Phys Chem B 103(16):3073–3077

Link S, Burda C, Nikoobakht B, El-Sayed MA (2000) Laser-induced shape changes of colloidal gold nanorods using femtosecond and nanosecond laser pulses. J Phys Chem B 104 (26):6152–6163

Liu M, Kono K, Fréchet JMJ (1999) Water-soluble dendrimer–poly(ethylene glycol) starlike conjugates as potential drug carriers. J Polym Sci A Polym Chem 37(17):3492–3503

Liu SY, Liang ZS, Gao F, Luo SF, Lu GQ (2010) In vitro photothermal study of gold nanoshells functionalized with small targeting peptides to liver cancer cells. J Mater Sci Mater Med 21 (2):665–674

Loo C, Lowery A, Halas N, West J, Drezek R (2005) Immunotargeted nanoshells for integrated cancer imaging and therapy. Nano Lett 5(4):709–711

Lu J, Zhou W, Wang L, Jia J, Ke Y, Yang L, Zhou K, Liu X, Tang Z, Li L, Chen S (2016) Core–shell nanocomposites based on gold nanoparticle@zinc–iron-embedded porous carbons derived from metal–organic frameworks as efficient dual catalysts for oxygen reduction and hydrogen evolution reactions. ACS Catal 6(2):1045–1053

Luo D, Haverstick K, Belcheva N, Han E, Saltzman WM (2002) Poly(ethylene glycol)-conjugated PAMAM dendrimer for biocompatible, high-efficiency DNA delivery. Macromolecules 35 (9):3456–3462

MacLellan CJ, Fuentes D, Elliott AM, Schwartz J, Hazle JD, Stafford RJ (2014) Estimating nanoparticle optical absorption with magnetic resonance temperature imaging and bioheat transfer simulation. Int J Hyperth 30(1):47–55

Madsen SJ, Angell-Petersen E, Spetalen S, Carper SW, Ziegler SA, Hirschberg H (2006) Photo-dynamic therapy of newly implanted glioma cells in the rat brain. Lasers Surg Med 38 (5):540–548

Madsen SJ, Baek S-K, Makkouk AR, Krasieva T, Hirschberg H (2012) Macrophages as cell-based delivery systems for nanoshells in photothermal therapy. Ann Biomed Eng 40(2):507–515

von Maltzahn G, Park JH, Agrawal A, Bandaru NK, Das SK, Sailor MJ, Bhatia SN (2009) Computationally guided photothermal tumor therapy using long-circulating gold nanorod antennas. Cancer Res 69(9):3892–3900

Manuchehrabadi N, Zhu L (2014) Development of a computational simulation tool to design a protocol for treating prostate tumours using transurethral laser photothermal therapy. Int J Hyperth 30(6):349–361

Manuchehrabadi N, Attaluri A, Cai H, Edziah R, Lalanne E, Bieberich C, Ma R, Johnson AM, Zhu L (2012) MicroCT imaging and in vivo temperature elevations in implanted prostatic tumors in laser photothermal therapy using gold nanorods. J Nanotechnol Eng Med 3(2):021003

Manuchehrabadi N, Chen Y, Lebrun A, Ma R, Zhu L (2013a) Computational simulation of temperature elevations in tumors using Monte Carlo method and comparison to experimental measurements in laser photothermal therapy. J Biomech Eng 135(12):121007

Manuchehrabadi N, Toughiri R, Bieberich C, Cai H, Attaluri A, Edziah R, Lalanne E, Johnson AM, Ma R, Zhu L (2013b) Treatment efficacy of laser photothermal therapy using gold nanorods. Int J Biomed Eng Technol 12(2):157–176

Martin CR (1994) Nanomaterials – a membrane-based synthetic approach. Office of Naval Research, contract N00014-82K-0612, technical report # 96

Melancon MP, Lu W, Yang Z, Zhang R, Cheng Z, Elliot AM, Stafford J, Olson T, Zhang JZ, Li C (2008) In vitro and in vivo targeting of hollow gold nanoshells directed at epidermal growth factor receptor for photothermal ablation therapy. Mol Cancer Ther 7(6):1730–1739

Mercatelli R, Ratto F, Centi S, Soria S, Romano G, Matteini P, Quercioli F, Pini R, Fusi F (2013) Quantitative readout of optically encoded gold nanorods using an ordinary dark-field microscope. Nanoscale 5(20):9645–9650

Meyers JD, Cheng Y, Broome A-M, Agnes RS, Schluchter MD, Margevicius S, Wang X, Kenney ME, Burda C, Basilion JP (2015) Peptide-targeted gold nanoparticles for photodynamic therapy of brain cancer. Part Part Syst Charact 32(4):448–457

Mie G (1908) Beiträge zur optik trüber medien, speziell kolloidaler metallösungen. Ann Phys 330 (3):377–445

Millstone JE, Park S, Shuford KL, Qin L, Schatz GC, Mirkin CA (2005) Observation of a quadrupole plasmon mode for a colloidal solution of gold nanoprisms. J Am Chem Soc 127 (15):5312–5313

Minkowycz W, Sparrow EM, Abraham JP (2012) Nanoparticle heat transfer and fluid flow, vol 4. CRC Press, New York

Moon H, Kumar D, Kim H, Sim C, Chang J-H, Kim J-M, Kim H, Lim D-K (2015) Amplified photoacoustic performance and enhanced photothermal stability of reduced graphene oxide coated gold nanorods for sensitive photoacoustic imaging. ACS Nano 9(3):2711–2719

Mooney R, Schena E, Zhumkhawala A, Aboody KS, Berlin JM (2015) Internal temperature increase during photothermal tumour ablation in mice using gold nanorods. The 37th annual international conference of the IEEE engineering in medicine and biology society (EMBC)

Moritz AR, Henriques F Jr (1947) Studies of thermal injury: II. The relative importance of time and surface temperature in the causation of cutaneous burns. Am J Pathol 23(5):695

Moroz P, Jones SK, Gray BN (2002) Magnetically mediated hyperthermia: current status and future directions. Int J Hyperth 18(4):267–284

Mourant JR, Fuselier T, Boyer J, Johnson TM, Bigio IJ (1997) Predictions and measurements of scattering and absorption over broadwavelength ranges in tissue phantoms. Appl Opt 36 (4):949–957

Murphy CJ, Sau TK, Gole AM, Orendorff CJ, Gao J, Gou L, Hunyadi SE, Li T (2005) Anisotropic metal nanoparticles: synthesis, assembly, and optical applications. J Phys Chem B 109 (29):13857–13870

Myroshnychenko V, Rodriguez-Fernandez J, Pastoriza-Santos I, Funston AM, Novo C, Mulvaney P, Liz-Marzan LM, Garcia de Abajo FJ (2008) Modelling the optical response of gold nanoparticles. Chem Soc Rev 37(9):1792–1805

Neilson BH, Rudie EN, Dann M (1994) Method for treating interstitial tissue associated with microwave thermal therapy. US Patent US 5,330,518

Ng KC, Cheng W (2012) Fine-tuning longitudinal plasmon resonances of nanorods by thermal reshaping in aqueous media. Nanotechnology 23(10):105602

Nield DA, Kuznetsov AV (2009) The Cheng–Minkowycz problem for natural convective boundary-layer flow in a porous medium saturated by a nanofluid. Int J Heat Mass Transf 52 (25–26):5792–5795

Niidome T, Yamagata M, Okamoto Y, Akiyama Y, Takahashi H, Kawano T, Katayama Y, Niidome Y (2006) PEG-modified gold nanorods with a stealth character for in vivo applications. J Control Release 114(3):343–347

Nikoobakht B, El-Sayed MA (2001) Evidence for bilayer assembly of cationic surfactants on the surface of gold nanorods. Langmuir 17(20):6368–6374

Nikoobakht B, El-Sayed MA (2003) Preparation and growth mechanism of gold nanorods (NRs) using seed-mediated growth method. Chem Mater 15(10):1957–1962

Noh MS, Lee S, Kang H, Yang J-K, Lee H, Hwang D, Lee JW, Jeong S, Jang Y, Jun B-H, Jeong DH, Kim SK, Lee Y-S, Cho M-H (2015) Target-specific near-IR induced drug release and photothermal therapy with accumulated Au/Ag hollow nanoshells on pulmonary cancer cell membranes. Biomaterials 45:81–92

Norman RS, Stone JW, Gole A, Murphy CJ, Sabo-Attwood TL (2008) Targeted photothermal lysis of the pathogenic bacteria, pseudomonas aeruginosa, with gold nanorods. Nano Lett 8(1):302–306

O'Neal DP, Hirsch LR, Halas NJ, Payne JD, West JL (2004) Photo-thermal tumor ablation in mice using near infrared-absorbing nanoparticles. Cancer Lett 209(2):171–176

Oldenburg SJ, Averitt RD, Westcott SL, Halas NJ (1998) Nanoengineering of optical resonances. Chem Phys Lett 288(2–4):243–247

Pan Y, Neuss S, Leifert A, Fischler M, Wen F, Simon U, Schmid G, Brandau W, Jahnen-Dechent W (2007) Size-dependent cytotoxicity of gold nanoparticles. Small 3(11):1941–1949

Pearce JA (2009) Relationship between Arrhenius models of thermal damage and the CEM 43 thermal dose. In: Proceedings of SPIE 7181, energy-based treatment of tissue and assessment, volume 718104

Pearce JA (2015) Improving accuracy in Arrhenius models of cell death: adding a temperature-dependent time delay. J Biomech Eng 137(12):121006

Pennes HH (1948) Analysis of tissue and arterial blood temperature in the resting human forearm. J Appl Phys 1:93–122

Peracchia MT, Fattal E, Desmaële D, Besnard M, Noël JP, Gomis JM, Appel M, d'Angelo J, Couvreur P (1999) Stealth® PEGylated polycyanoacrylate nanoparticles for intravenous administration and splenic targeting. J Control Release 60(1):121–128

Pérez-Juste J, Pastoriza-Santos I, Liz-Marzán LM, Mulvaney P (2005) Gold nanorods: synthesis, characterization and applications. Coord Chem Rev 249(17–18):1870–1901

Piao DBJZ, Bartels KE, Holyoak GR, Ritchey JW, Xu G, Bunting CF, Slobodov G (2009) In vivo transrectal ultrasound coupled near-infrared optical tomography of intact normal canine prostate. J Innov Opt Health Sci 2(3):215–225

Piao DBBK, Jiang Z, Holyoak GR, Ritchey JW, Xu G, Bunting CF, Slobodov G (2010) Alternative transrectal prostate imaging: a diffuse optical tomography method. IEEE J Sel Top Quantum Electron 16(4):715–729

Pissuwan D, Valenzuela SM, Killingsworth MC, Xu X, Cortie MB (2007a) Targeted destruction of murine macrophage cells with bioconjugated gold nanorods. J Nanopart Res 9(6):1109–1124

Pissuwan D, Valenzuela SM, Miller CM, Cortie MB (2007b) A golden bullet? Selective targeting of toxoplasma gondii tachyzoites using antibody-functionalized gold nanorods. Nano Lett 7 (12):3808–3812

Qin Z, Balasubramanian SK, Wolkers WF, Pearce JA, Bischof JC (2014) Correlated parameter fit of Arrhenius model for thermal denaturation of proteins and cells. Ann Biomed Eng 42 (12):2392–2404

Raaymakers B, Kotte A, Lagendijk J, Minkowycz W, Sparrow E, Abraham J (2009) Discrete vasculature (DIVA) model simulating the thermal impact of individual blood vessels for in vivo heat transfer. Adv Numer Heat Tran 3:121–148

Roberts MJ, Bentley MD, Harris JM (2012) Chemistry for peptide and protein PEGylation. Adv Drug Deliv Rev 64(Suppl):116–127

Rodrigues HF, Mello FM, Branquinho LC, Zufelato N, Silveira-Lacerda EP, Bakuzis AF (2013) Real-time infrared thermography detection of magnetic nanoparticle hyperthermia in a murine model under a non-uniform field configuration. Int J Hyperth 29(8):752–767

Rudie EN, Neilson BH, Kauphusman JV (1996) Device for asymmetrical thermal therapy with helical dipole microwave antenna. US Patent 5,545,137

Ryu S, Brown SL, Kim S-H, Khil MS, Kim JH (1996) Preferential radiosensitization of human prostatic carcinoma cells by mild hyperthermia. Int J Radiat Oncol Biol Phys 34(1):133–138

Salem AK, Searson PC, Leong KW (2003) Multifunctional nanorods for gene delivery. Nat Mater 2 (10):668–671

Sapareto SA, Dewey WC (1984) Thermal dose determination in cancer therapy. Int J Radiat Oncol Biol Phys 10(6):787–800

Schwartz JA, Shetty AM, Price RE, Stafford RJ, Wang JC, Uthamanthil RK, Pham K, McNichols RJ, Coleman CL, Payne JD (2009) Feasibility study of particle-assisted laser ablation of brain tumors in orthotopic canine model. Cancer Res 69(4):1659–1667

Shenoy D, Fu W, Li J, Crasto C, Jones G, DiMarzio C, Sridhar S, Amiji M (2006) Surface functionalization of gold nanoparticles using hetero-bifunctional poly(ethylene glycol) spacer for intracellular tracking and delivery. Int J Nanomedicine 1(1):51–57

Sherar MD, Gertner MR, Yue CK, O'Malley ME, Toi A, Gladman AS, Davidson SR, Trachtenberg J (2001) Interstitial microwave thermal therapy for prostate cancer: method of treatment and results of a phase I/II trial. J Urol 166(5):1707–1714

Shoshan-Barmatz V, Israelson A, Brdiczka D, Sheu SS (2006) The voltage-dependent anion channel (VDAC): function in intracellular signalling, cell life and cell death. Curr Pharm Des 12(18):2249–2270

Skrabalak SE, Chen J, Sun Y, Lu X, Au L, Cobley LM, Xia Y (2008) Gold nanocages: synthesis, properties, and applications. Acc Chem Res 41(12):1587–1595

Sönnichsen C, Franzl T, Wilk T, Plessen GV, Feldmann J (2002) Plasmon resonances in large noble-metal clusters. New J Phys 4(1):93

Stafford RJ, Shetty A, Elliott AM, Schwartz JA, Goodrich GP, Hazle JD (2011) MR temperature imaging of nanoshell mediated laser ablation. Int J Hyperth 27(8):782–790

Stern JM, Stanfield J, Kabbani W, Hsieh JT, Cadeddu JA (2008) Selective prostate cancer thermal ablation with laser activated gold nanoshells. J Urol 179(2):748–753

Stern JM, Kibanov Solomonov VV, Sazykina E, Schwartz JA, Gad SC, Goodrich GP (2016) Initial evaluation of the safety of nanoshell-directed photothermal therapy in the treatment of prostate disease. Int J Toxicol 35(1):38–46

Takahashi H, Niidome Y, Niidome T, Kaneko K, Kawasaki H, Yamada S (2006) Modification of gold nanorods using phosphatidylcholine to reduce cytotoxicity. Langmuir 22(1):2–5

Tasciotti E, Liu X, Bhavane R, Plant K, Leonard AD, Price BK, Cheng MM-C, Decuzzi P, Tour JM, Robertson F, Ferrari M (2008) Mesoporous silicon particles as a multistage delivery system for imaging and therapeutic applications. Nat Nanotechnol 3(3):151–157

Tong L, Zhao Y, Huff TB, Hansen MN, Wei A, Cheng JX (2007) Gold nanorods mediate tumor cell death by compromising membrane integrity. Adv Mater 19(20):3136–3141

Tong L, Wei Q, Wei A, Cheng JX (2009) Gold nanorods as contrast agents for biological imaging: optical properties, surface conjugation and photothermal effects. Photochem Photobiol 85(1):21–32

Tuchin VV (2015) Tissue optics, light scattering methods and instruments for medical diagnostics. Spie Press Book, Bellingham

Vafai K (2015) Handbook of porous media. CRC Press, Boca Raton

Verhaart RF, Verduijn GM, Fortunati V, Rijnen Z, van Walsum T, Veenland JF, Paulides MM (2015) Accurate 3D temperature dosimetry during hyperthermia therapy by combining invasive measurements and patient-specific simulations. Int J Hyperth 31(6):686–692

Vogel A, Venugopalan V (2003) Kinetics of phase transitions in pulsed IR laser ablation of biological tissues. In: Proceedings of SPIE Vol. 4961 laser tissue interaction XIV, pp 66–74

Wang L, Jacques SL, Zheng L (1995) MCML – Monte Carlo modeling of light transport in multi-layered tissues. Comput Methods Prog Biomed 47(2):131–146

Wang B-K, Yu X-F, Wang J-H, Li Z-B, Li P-H, Wang H, Song L, Chu PK, Li C (2016) Gold-nanorods-siRNA nanoplex for improved photothermal therapy by gene silencing. Biomaterials 78:27–39

Welch AJ, van Gemert MJC (1995) Optical-thermal response of laser-irradiated tissue. Plenum Press, New York

Werthmöller N, Frey B, Rückert M, Lotter M, Fietkau R, Gaipl US (2016) Combination of ionising radiation with hyperthermia increases the immunogenic potential of B16-F10 melanoma cells in vitro and in vivo. Int J Hyperth 32(1):23–30

Westcott SL, Oldenburg SJ, Lee TR, Halas NJ (1998) Formation and adsorption of clusters of gold nanoparticles onto functionalized silica nanoparticle surfaces. Langmuir 14(19):5396–5401

Wilson BC, Adam G (1983) A Monte Carlo model for the absorption and flux distributions of light in tissue. Med Phys 10(6):824–830

Wong SL, Mangu PB, Choti MA, Crocenzi TS, Dodd GD 3rd, Dorfman GS, Eng C, Fong Y, Giusti AF, Lu D, Marsland TA, Michelson R, Poston GJ, Schrag D, Seidenfeld J, Benson AB 3rd (2010) American Society of Clinical Oncology 2009 clinical evidence review on radiofrequency ablation of hepatic metastases from colorectal cancer. J Clin Oncol 28(3):493–508

Wulff W (1974) The energy conservation equation for living tissue. IEEE Trans Biomed Eng 6 (BME-21):494–495

Yang H-W, Liu H-L, Li M-L, Hsi IW, Fan C-T, Huang C-Y, Lu Y-J, Hua M-Y, Chou H-Y, Liaw J-W, Ma C-CM, Wei K-C (2013) Magnetic gold-nanorod/ PNIPAAmMA nanoparticles for dual magnetic resonance and photoacoustic imaging and targeted photothermal therapy. Biomaterials 34(22):5651–5660

Yavuz MS, Cheng Y, Chen J, Cobley CM, Zhang Q, Rycenga M, Xie J, Kim C, Song KH, Schwartz AG, Wang LV, Xia Y (2009) Gold nanocages covered by smart polymers for controlled release with near-infrared light. Nat Mater 8(12):935–939

Ye D, Wang G, Liu Y, Huang W, Wu M, Zhu S, Jia W, Deng A-M, Liu H, Kang J (2012) MiR-138 promotes induced pluripotent stem cell generation through the regulation of the p53 signaling. Stem Cells 30(8):1645–1654

Ying Y, Chang S-S, Lee C-L, Wang CRC (1997) Gold nanorods: electrochemical synthesis and optical properties. J Phys Chem B 101(34):6661–6664

Zaman RT, Diagaradjane P, Wang JC, Schwartz J, Rajaram N, Gill-Sharp KL, Cho SH, Rylander HG III, Payne JD, Krishnan S (2007) In vivo detection of gold nanoshells in tumors using diffuse optical spectroscopy. IEEE J Sel Top Quantum Electron 13(6):1715–1720

Zhang G, Yang Z, Lu W, Zhang R, Huang Q, Tian M, Li L, Liang D, Li C (2009) Influence of anchoring ligands and particle size on the colloidal stability and in vivo biodistribution of polyethylene glycol-coated gold nanoparticles in tumor-xenografted mice. Biomaterials 30 (10):1928–1936

Zhang W, Meng J, Ji Y, Li X, Kong H, Wu X, Xu H (2011) Inhibiting metastasis of breast cancer cells in vitro using gold nanorod-siRNA delivery system. Nanoscale 3(9):3923–3932

Zhang W, Ji Y, Wu X, Xu H (2013) Trafficking of gold nanorods in breast cancer cells: uptake, lysosome maturation, and elimination. ACS Appl Mater Interfaces 5(19):9856–9865

Zhang J, Li C, Zhang X, Huo S, Jin S, An F-F, Wang X, Xue X, Okeke CI, Duan G, Guo F, Zhang X, Hao J, Wang PC, Zhang J, Liang X-J (2015) In vivo tumor-targeted dual-modal fluorescence/CT imaging using a nanoprobe co-loaded with an aggregation-induced emission dye and gold nanoparticles. Biomaterials 42:103–111

Zhang N, Chen H, Liu A-Y, Shen J-J, Shah V, Zhang C, Hong J, Ding Y (2016a) Gold conjugate-based liposomes with hybrid cluster bomb structure for liver cancer therapy. Biomaterials 74:280–291

Zhang W, Wang F, Wang Y, Wang J, Yu Y, Guo S, Chen R, Zhou D (2016b) pH and near-infrared light dual-stimuli responsive drug delivery using DNA-conjugated gold nanorods for effective treatment of multidrug resistant cancer cells. J Control Release 232:9–19

Zou YPLW, Zheng F, Li FC, Huang H, Du JD, Liu HR (2010) Intraoperative radiofrequency ablation combined with 125iodine seed implantation for unresectable pancreatic cancer. World J Gastroenterol 16(40):5104–5110